Opportunistic Schedule Selection for Multiuser MIMO FSO Communications: A Security-Reliability Trade-Off Perspective

Wafaa Mohammed Ridha Shakir, *Member, IEEE*, Jinan Charafeddine, *Student Member, IEEE*, Haitham Al Satai, Hani Hamdan, Samir Haddad, and Jinane Sayah

***Abstract*—The security and reliability of free space optical (FSO) communications and the trade-off between the two are the most critical characteristics to emphasize in FSO systems, especially as optical wireless communications continue to evolve. In this work, we investigate the impact of opportunistic transmit aperture selection (TAS) on the security-reliability trade-off (SRT) of the multiuser multiple-input multiple-output (MU-MIMO) free space optical system. We consider a general scenario in which the FSO system consists of a transmitter side with K users and a single receiver with N apertures communicating over generalized Malaga-M turbulence channels. We derive the TAS combined signal-to-noise ratio (SNR) distributions for the FSO MIMO channel between the transmitting users and the receiver. A statistical analysis of the TAS scheme is performed, where the kth best user with the highest SNR is selected. Based on this analysis, the closed-form expressions for the outage probability, average bit error rate, intercept probability, and SRT are derived. Then, the diversity advantages provided by the channel variations considering the atmospheric turbulence and generalized nonzero boresight pointing errors are further discussed. The results show that the considered TAS significantly improves the security, reliability, and SRT performance and has the potential to solve existing FSO communication problems. Monte Carlo simulations are used to verify the correctness of the numerical results.**

***Index Terms*—Free space optical, security, reliability, security-reliability trade-off, opportunistic scheduling selection, transmit aperture selection, atmospheric turbulence, nonzero boresight pointing errors, multiple-input–multiple-output.**

Manuscript received 27 January 2023; revised 12 March 2023; accepted 23 March 2023. Date of publication 27 March 2023; date of current version 21 April 2023. *(Corresponding author: Wafaa Mohammed Ridha Shakir.)*

Wafaa Mohammed Ridha Shakir is with the Computer Systems Department, Al-Furat Al-Awsat Technical University, Babil 51015, Iraq (e-mail: inb.wfa@atu.edu.iq).

Jinan Charafeddine and Haitham Al Satai are with the Pôle scientifique et technologique de Vélizy, Laboratoire d'Ingénierie des Systèmes de Versailles (LISVEA4048), Université Paris-Saclay, 78140 Vélizy, France (e-mail: jinan.charafeddine@lisv.uvsq.fr; haitham.al-satai@uvsq.fr).

Hani Hamdan is with the CentraleSupélec, CNRS, Laboratoire des Signaux et Systèmes (L2S UMR CNRS 8506), Université Paris-Saclay 91190 Gif-sur-Yvette, France (e-mail: hani.hamdan@centralesupelec.fr).

Samir Haddad is with the Department of Computer Science and Mathematics, Faculty of Arts and Sciences, University of Balamand, Koura 3936, Lebanon (e-mail: samir.haddad@balamand.edu.lb).

Jinane Sayah is with the Department of Telecom and Networks, Issam Fares Faculty of Technology, University of Balamand, Koura 3936, Lebanon (e-mail: jinane.sayah@balamand.edu.lb).

Digital Object Identifier 10.1109/JPHOT.2023.3262183

I. Introduction

GLOBAL mobile traffic is expected to increase 670 times by 2030, driven by advanced technological devices and real-time applications with massive bandwidth [1]. In this way, security issues in wireless communication systems have attracted considerable attention at present and in the future. Moreover, this great interest in security issues of communication networks is expected to increase in the coming years with the emerging implementation of 5G and beyond networks. Secure transmission in the presence of an external eavesdropper is a significant research problem in communication networks. In this scenario, legitimate users want to send confidential messages to the legitimate recipient without being overheard by the eavesdropper [2]. Compared to the already congested radio frequency (RF) spectrum, free space optical (FSO) communication enables license-free operation, low costs, and high-data-rate transmission, all of which are critical in various application scenarios. The absence of licensing fees and regulatory restrictions on bandwidth consumption highlights the effectiveness of FSO communications as a backup solution for disaster recovery and military applications [3]. FSO systems initially attracted attention as an efficient solution to the "last mile" problem, bridging the gap between the end user and the existing fiber optic infrastructure. Connectivity between buildings, video surveillance, backhaul for cellular networks, IoT, and satellite communications are some attractive applications of FSO communications [4]. For this reason, there is growing interest in privacy and security issues of FSO communication systems in the presence of an external eavesdropper that can extract information from the legitimate transmission. In general, FSO is more secure than RF communications due to the high directionality of the laser beam. However, according to recent research on wireless optical systems, FSO communications are not interception-free at the physical layer, especially when the laser beam's main lobe is significantly larger than the receiver's size [5], [6], [7]. A plausible mechanism for interception is the reflection of some of the beam radiation by small particles and subsequent detection by an eavesdropper not in the line-of-sight (LOS) of both communication peers. In another scenario, the eavesdropper would block the laser beam to collect some of the optical energy. Since the laser beam diverges due to optical diffractions, one strategy for successful eavesdropping is to position the eavesdropper

in the beam's divergence region. Regarding long-distance FSO communication, the eavesdropper can intercept the FSO link better by collecting the power that legitimate peers do not capture [2]. An optical beam transmitted with a small divergence angle of 1 mrad might have a radius of 1 m over a 1 km transmission distance. Consequently, physical layer security (PLS) is emerging as a promising secure wireless communications paradigm relying on exploiting the physical characteristics of wireless channels for protection against eavesdropping attacks. Contrary to the cryptographic techniques with highly complex encryption methods, which require more processing resources for encryption and decryption and increase the latency imposed, PLS takes advantage of the inherent randomness of wireless channels to secure communications between legitimate peers [8], [9]. PLS can be considered the most secure method of communication since security in this context is provable (in the information-theoretic sense). For example, in a typical wiretap model, PLS theory states that secure communication is possible if the capacity of the legitimate channel is higher than that of the eavesdropping channel. Motivated by the PLS schemes of RF systems, various PLS techniques have been proposed to secure FSO communications, such as diversity approaches [10], [11], transmit aperture selection (TAS) [12], artificial noise injection [13], and generalized chaotic modulation [14]. However, many characteristics of FSO systems differ from RF systems (e.g., the channel, and the physical characteristics of the transmitting and receiving devices). Therefore, these differences must be taken into account when adapting PLS techniques to FSO systems. A number of studies have considered these unique properties. For example, Lopez-Martinez et al. [15] characterized the PLS in single-input single-output (SISO) FSO transmissions in the presence of an eavesdropper. Due to the effects of both laser beam divergence and turbulence-induced fading, they discussed possible eavesdropping mechanisms. They concluded that the eavesdropper can interfere with communications when it is close to the legitimate receiver or transmitter. Saber and Sadough [16] evaluated the secure performance of the SISO FSO link over Malaga-M turbulence channels. Later, Verma et al. [17] evaluated the impact of nonzero boresight pointing errors on secrecy performance for the same system in [16]. Furthermore, Monteiro et al. evaluated the effective secrecy throughput (EST) of an FSO system consisting of a multiple-aperture transmitter, a multiple-aperture receiver, and a multiple-aperture eavesdropper in [18]. They showed that the use of multiple apertures on the transmitter is crucial to approach the optimal EST. Moreover, Han et al. in [19] analyzed the secrecy performance of the SISO FSO link over the F-distribution turbulence with pointing error effects.

On one hand, there is no doubt that the reliability of FSO systems is vulnerable to path loss, misalignment, and atmospheric turbulence, which can seriously limit FSO transmissions at shorter distances [20]. On the other hand, despite capacity increments created by new technologies including FSO, mobile operators still struggle to meet user demands. A viable alternative to bandwidth expansion is to allocate the available bandwidth optimally, or at least more efficiently. The basic idea of opportunistic scheduling selection (OSS) is to exploit channel variations to schedule a user with the best channel conditions at a given time [21]. The contemporary standard that employs OSS includes WiMAX [22]. OSS is the function responsible for resource allocation between users, and its role is to decide which user should transmit/receive and when, and therefore affects the efficiency of bandwidth utilization. The gain is primarily due to multiuser diversity, which views channel fading as an opportunity rather than an obstacle: When selecting one user out of many, it is almost always possible to select one that is above the "average." Therefore, users in fading areas are typically not served [21]. An example of an opportunistic method is the transmit aperture selection, which is based on selecting a path with the highest value of irradiance or fading gain to counteract fading and improve performance [23].

Additionally, it is shown in several studies that as the intercept probability (P_{int}) (which considers a system's security metric) requirement is relaxed, the outage probability (P_{out}) (considered as reliability metric) performance improves, and vice versa [24], [25]. This implies a trade-off between the security and reliability of the wireless transmission in the presence of eavesdropping attacks, which is referred to as the security-reliability trade-off (SRT). Although the notion of SRT was studied in the context of FSO transmission [26], [27], these contributions were mainly focused on the employment of encryption algorithms to protect against eavesdropping attacks. By contrast, in our work, PLS- rather than encryption techniques - is invoked for characterizing the SRT attained in MIMO environments with the help of OSS schemes for enhancing the multiuser FSO system performance.

A. Related Work

Next, we are going to elaborate on the applications of opportunistic scheduling selection in FSO communication systems according to several fields that researchers have identified. These fields fall broadly into the following categories:

1) Diversity Techniques: Scanning the literature, there have been studies on employing opportunistic selection scheduling to improve the FSO systems' diversity gain and reduce the influence of wireless channel impurities. In this context, Abouei and Plataniotis investigated several OSS schemes for varying degrees of the trade-off between throughput and fairness between users across a log-normal (weak) turbulence channels for multiuser MIMO (MU-MIMO) FSO system assuming non-equidistant user placement [28]. Yang et al. evaluated the performance of a multiuser single-input multiple-output (MU-SIMO) FSO system with the best user selection (BUS) scheme over weak (log-normal) and strong (Gamma-Gamma) turbulence channels [29]. They do, however, assume a constant average signal-to-noise ratio (SNR) for all users. This implies that path loss effects are either disregarded or that each user is positioned equidistant from the central node, resulting in identical path loss. Such an assumption is unrealistic because users in a real-world system are likely to be spread out over a broad area. Furthermore, unlike RF systems, the fading variance in FSO systems is distance-dependent [12]; hence user placement has a significant influence on multiuser system performance.

Zhalehpour and Uysal developed an accurate analysis for the outage capacity of several scheduling schemes including in an MU-MIMO FSO system over a weak turbulence channel [30]. Later, they extended the analysis to the outage throughput of the system [31] considering the same channel model in [30]. However, the consequences of path loss and pointing errors are ignored in [28], [29], [30], and [31].

2) Reliability Performance Enhancement: Another group of studies investigated OSS for improving the FSO systems' reliability [32], [33], [34], [35], [36], [37], [38], [39], [40]. Qin et al. analyzed the outage probability of the MU-MIMO FSO transmission over Gamma-Gamma atmospheric turbulence using repetition coding (RC) and transmit laser selection (TLS) schemes [32]. To circumvent this, the end-to-end SNR of the MIMO FSO channel is approximated since the exact closed-form expression for such a channel is remarkably complex and not easily tractable due to the complication of its statistics. This approximation method was first considered in [41] to approximate the MIMO FSO transmission over the Gamma-Gamma environment. Cherif et al. examined the effect of interference on the performance of multi apertures-multiuser (MA-MU) mixed FSO/RF relay networks with Malaga-M/Nakagami-m distributions [33]. To select between FSO apertures at the relay node, transmit aperture selection scheme was used. While the BUS was used on the RF link to select between users over the RF link. However, the pointing errors and path loss did not consider in [32], [33], and [41]. Salhab et al. employed MU-MISO mixed RF/FSO relay network with a BUS scheme in RF link to enhance the system reliability over Rayleigh/Gamma-Gamma fading channels [34]. Similar studies for mixed RF/FSO relay systems can be found in [35], [36], [37], [38], [39]. The Gamma-Gamma distribution characterized the SISO FSO link in [34], [35], [36], [37], [38], [39], while the Malaga-M distribution is chosen to represent the multi aperture FSO links with asymptotic analysis in [33]. Michailidis et al. introduced a hovering unmanned aerial vehicle (UAV) that served as a decode and forward relay (DF) between the ground central unit (CU) and multiple ground users (GU) for mixed FSO/RF system over log-normal/Nakagmi-IG fading channels in another study [40]. For the FSO, the TAS scheme is explored for opportunistic selection, while opportunistic GU scheduling (GUS) is used in the RF links to improve the system's outage probability [40].

3) Security Performance Enhancement: An additional group of studies explored the OSS for improving the security performance of the mixed RF/FSO and FSO systems against eavesdropping attacks [12], [42], [43], [44]. For example, Abd El-Malek et al. investigated the security of MU-SIMO mixed RF-FSO relay networks by employing the BUS scheme in the multiuser RF link [42]. They also looked at the effect of eavesdropper attacks in RF links on the security of the system. Later, in another study, they evaluate the influence of RF co-channel interference (CCI) on the SRT for the same system [43]. Additionally, they employed power allocation and cooperative jamming techniques to enhance the system's security performance [43]. However, the SISO FSO link with Gamma-Gamma distribution is considered as an extension for the multiuser RF link in all these studies [42], [43], [44]. Finally, Shakir [12] examined the security performance of the MISO FSO networks adopting the BUS scheme. The Malaga-M turbulence is used to characterized the FSO channel with the same approximation method for the channel model adopted in [33].

Analyzing the above and related literature, we find some research gaps in the study of the security-reliability trade-off of the FSO system based on OSS, which need to be addressed. Firstly, the pointing error loss was ignored or limited to zero boresight in FSO transmission. The nonzero boresight model generalizes the effect of pointing errors on the FSO transmission. However, although the statistical analysis of nonzero boresight pointing errors for the FSO system has been investigated extensively in the literature, it has yet to be addressed in the context of SRT for the MU-MIMO FSO systems.

Second, for atmospheric turbulence, lognormal models for weak turbulence or Gamma-Gamma models for strong and moderate turbulence were mostly used. It is worth noting that the SISO FSO transmission utilizing the general Malaga-M distribution to characterize atmospheric turbulence, has been intensively studied in many works in the literature to evaluate the performance of the FSO system over a wide range of turbulence conditions [45], [46]. However, very few works [12] have used the Malaga-M distribution in the multiuser FSO environment in the context of SRT due to the high complexity of the mathematical formulation of such systems.

According to the Malaga-M model, the small-scale fading characteristics of the atmospheric channel are modeled by three different signal components. Thus, the received irradiance contributes to a LOS field component and two scattered optical field components due to the small-scale fluctuations. The first of these two scattered components is the quasi-forward optical signal scattered by eddies on the propagation axis, which is assumed to be coupled to the LOS component. The second component is the classical optical scattered field, which is due to the energy scattered by the off-axis eddies and is statistically independent of the other two components. The inclusion of the component coupled to the LOS scattering component is the main novelty of the model and can be justified by the high directivity and narrow beamwidths of laser beams in atmospheric optical communications [45].

As mentioned earlier, the Malaga-M distribution is a significant model for the FSO channel because it accurately models the irradiance fluctuations in a closed mathematical expression over a wide range of turbulence conditions, i.e., from weak to strong. Another significant advantage of the Malaga-M distribution is that it generalizes other known distributions to adequately model the ever-changing atmospheric turbulence conditions, as it agrees well with experimental results [47]. In Table I of [47], it was shown that various distributions such as the Rice-Nakagami, the Gamma-Gamma, the Shadowed-Rician, the K-distribution, the homodyned-K, the exponential, the Gamma-Rician distribution, etc., can be constructed from the Malaga-M distribution. However, the Malaga-M distribution is represented by the modified Bessel function of the second kind. Therefore, it is very challenging and complicated to analyze the SRT of the MIMO FSO systems. To the best of the authors' knowledge, there are no analyses for the trade-off between security and reliability for the MU-MIMO FSO system considering the Malaga-M atmospheric turbulence.

TABLE I
LIST OF NOTATIONS

$X^i_{1,k} \triangleq \frac{C^i_1(0)_k(v_i)^{\varphi_e^2+k}}{k!\,\Gamma(k+1-\alpha_e+\varphi_e^2)\Gamma(k+1-j+\varphi_e^2)}; \Omega^i_{1,k} = \frac{\varphi_e^2+k}{2}$
$X^i_{2,p} \triangleq \frac{C^i_2(\alpha_e-\varphi_e^2)_p(v_i)^{\alpha_e+p}}{p!\,\Gamma(p+1-\varphi_e^2+\alpha_e)\Gamma(p+1-k+\alpha_e)};\ \Omega_{2,p} = \frac{\alpha_e+p}{2}$
$X^i_{3,q} \triangleq \frac{C^i_3(j-\varphi_e^2)_q(v_i)^{j+q}}{q!\,\Gamma(q+1-\varphi_e^2+k)\Gamma(q+1-\alpha_e+j)}; \Omega_{3,q} = \frac{j+q}{2}$
$C^i_1 = \frac{csc\left(\pi(\alpha_e-\varphi_e^2)\right)csc\left(\pi(j-\varphi_e^2)\right)}{\Gamma(1)};$
$C^i_2 = \frac{csc\left(\pi(\varphi_e^2-\alpha_e)\right)csc(\pi(j-\alpha_e))}{\Gamma(\varphi_e^2+1-\alpha_e)};$
$C^i_3 = \frac{csc\left(\pi(\varphi_e^2-j)\right)csc(\pi(\alpha_e-j))}{\Gamma(\varphi_e^2+1-j)};\ v_i \triangleq \frac{\alpha_e\beta_e}{\delta\beta_e+\Omega'}\sqrt{\frac{1}{\gamma_e}},\ B_e = \frac{\alpha_e\beta_e}{(g\beta_e+\hat{\Omega})}$
$\tau = \sum_{k=0}^{MP-1}\Omega_{1,k} + \sum_{p=0}^{MP-1-k_e}\Omega_{1,p} + \sum_{q=0}^{MP-1-k_e-r}\Omega_{1,q}$

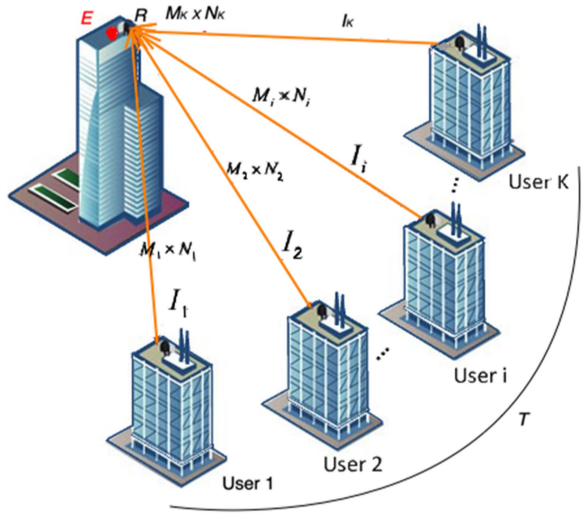

Fig. 1. A multiuser MIMO FSO communication system model depicting the transmit users, receiver, and an eavesdropper.

B. Motivation and Contributions

Despite their considerable potential as excellent candidates for future backhaul networks and various other applications, the SRT of MU-MIMO FSO systems has not yet been studied in depth in the open literature, using an OSS scheme to improve both the security and reliability of these systems. At the same time, most related research focuses on implementing the OSS to improve the performance of the multiuser RF link's performance of the mixed RF/FSO systems regardless of the FSO link. In contrast to previous studies of comparable systems [42], [43], [44], we develop an SRT based on the TAS scheme for the MU-MIMO FSO systems using a generalized channel model. The chosen channel model makes it easy to understand how different system and channel parameters affect the systems' security, reliability, and SRT performance. Additionally, this paper presents a comprehensive analysis of the TAS-based opportunistic scheduling to improve the SRT performance of MU-MIMO FSO systems. The main contributions of this paper can be summarized as follows:

1) We first develop the probability density function (PDF) and cumulative distribution function (CDF) of the MU-MIMO FSO system with the TAS and consider the generalized Malaga-M distribution with nonzero boresight pointing errors to make the study more realistic.
2) The exact and asymptotic analytical expressions of the outage probability are obtained to provide insightful information about the reliability performance of the system under investigation.
3) The exact and asymptotic analytical expressions of the average bit error rate (BER) are obtained to provide insightful information about the general performance of the considered system.
4) An exact and asymptotic analysis of the intercept probability, the primary metric for system security and SRT in the presence of an eavesdropper, was evaluated. To obtain the SRT of the system, we adopt a definition that also takes into account the predetermined outage threshold for the first time in such systems.
5) These expressions are used to generate numerical results with specified figures. In addition, Monte Carlo simulations verify the accuracy of the analytical results.

The following is the outline for this paper: Section II presents models of the MU-MIMO FSO system and channel in consideration, while Section III develops an analytical expression for the statistical analysis of TAS opportunistic scheduling for the considered system. Section IV considers the outage probability and the average BER analysis of the investigated system. Section V presents the secrecy performance analysis based on the intercept probability. The SRT of the considered system is discussed in Section VI. Section VII has several interesting numerical examples as well as informative discussions. Finally, Section VIII brings the paper to a conclusion.

II. System and Channel Models

We consider an MU-MIMO FSO communication system consisting of a transmitter T with K user groups equipped with M_i transmitting apertures that communicate with a receiver R equipped with N_i apertures over legitimate $T \rightarrow R$ links, where $i \in \{1, 2, \ldots, K\}$. A single unauthorized passive eavesdropper E equipped with P_t transmit apertures attempts to intercept confidential information over the unauthorized $T \rightarrow E$ links, where $t \in \{1, 2, \ldots, P\}$, E is located in the same receiving plane as R in this work. We assume that the transmit apertures of the ith user on the transmitter T are directed to the ith apertures of the receiver R, whose receive apertures are also directed to the transmit apertures of the ith user. Therefore, the transmitting users communicate with the ith receiver aperture through $M_i \times N_i$ MIMO FSO links, as shown in Fig. 1. For this system, the K groups of users are alternate in a time division. Considering the signal transmission between the mth transmitting user and the nth receiving aperture over the $T \rightarrow R$ links of the ith user, where $m \in \{1, 2, \ldots, M_i\}$, and $n \in \{1, 2, \ldots, N_i\}$, the received signal y^{mn}_{ir} at R can be written as

$$y^{mn}_{ir} = \eta G_{ir} I^{mn}_{ir} x_i + w^{mn}_{ir} \tag{1}$$

where η is the effective optical-to-electrical conversion ratio, I_{ir}^{mn} is the irradiance of the link between the mth transmitting user and the nth receiving aperture, x_i is the optical signal transmitted from the ith user to R, and w_{ir}^{mn} is the additive white Gaussian noise with zero mean and variance $N_o/2$. In this work, we assume the distance d_i between the ith user and the receiver R, while $\bar{d}$ represents the average distance between all users and R.

The path gain factor can be written as $G_{ir} = \left(\frac{\bar{d}}{d_i}\right)^2 e^{-\alpha_a(d_i-\bar{d})}$, where α_a is the atmospheric attenuation coefficient [32]. Moreover, atmospheric attenuation is caused by both molecular absorption and scattering of aerosols, suspended in the air. The total channel attenuation is given as $\alpha_a = \frac{A}{\pi(\frac{\vartheta d_i}{2})^2}\, exp(-\beta_v d_i)$, where $A = \pi D^2/4$, ϑ and β_v are the area of the receive aperture (with D denoting the receiver aperture diameter), the divergence angle of the optical beam in radian, and the atmospheric extinction coefficient, respectively [48].

According to the Malaga-M model, the probability density function of the normalized irradiance $f_{I_{ir}^{mn}}$ is derived in [47] as

$$f_{I_{ir}^{mn}}(I) = A_r \sum_{j=1}^{\beta_r} a_{jr}\, I^{\frac{\alpha_r+j}{2}-1}\, k_{\alpha_r-j} \times \left(2\sqrt{\frac{\alpha_r\beta_r I}{g\beta_r+\Omega^{'}}}\right),\ I>0 \tag{2}$$

where

$$A_r \triangleq \frac{2\alpha_r^{\alpha_r/2}}{g^{1+\alpha_r/2}\Gamma(\alpha_r)}\left(\frac{g\beta_r}{g\beta_r+\Omega'}\right)^{\beta_r+\alpha_r/2};$$

$$a_{jr} \triangleq \binom{\beta_r-1}{j-1}\frac{(g\beta_r+\Omega')^{1-\frac{j}{2}}}{(j-1)!}\left(\frac{\Omega'}{g}\right)^{j-1}\left(\frac{\alpha_r}{\beta_r}\right)^{\frac{j}{2}}, \tag{3}$$

$k_{\alpha_r-j}(\cdot)$ is the modified Bessel function of the second kind and order α_{r-j}, $\Gamma(\cdot)$ is the gamma function, $g = 2b_o(1-\rho)$ denotes the average power of the scattering component received by off-axis eddies, $2b_o$ is the average power for the component, which is quasi-forward scattered by the eddies on the propagation axis, and the component due to energy which is scattered to the receiver by off-axis eddies. Moreover, $0 \le \rho \le 1$ is the factor that represents the scattering power associated with the LOS component. The parameter Ω' indicates the average power of the LOS component. The parameters α_r and β_r are two parameters related to the atmospheric conditions on the legitimate $T \to R$ links and can be written as [49]

$$\alpha_r = \left[\exp\left(0.49\delta_r^2/(1+1.11\,\delta_r^2)^{7/6}\right)-1\right]^{-1} \tag{4}$$

$$\beta_r = \left[\exp\left(0.51\delta_r^2/(1+0.69\,\delta_r^2)^{5/6}\right)-1\right]^{-1} \tag{5}$$

where δ_r^2 is the Rytov variance, which is the function of the link distance d_i, the optical wave number k, and the refractive index structure constant C_n^2 and can be given by $\delta_r^2 = 1.23C_n^2k^{7/6}d_i^{11/6}$.

A. Channel Assumptions

If E is close to R on the same receiving plane, it is reasonable to assume that the optical irradiance I and atmospheric attenuation α_a parameters are the same for the links of R and E over a long transmission distance. To ensure that there is no turbulence-induced fading correlation, i.e., independence between the legitimate and intercepting links, the distance between the receivers of R and E should be sufficiently large. In this work, with the help of [49, Eq. (4)] that separation distances of at least 11, 17, and 20 cm are required to ensure channel independence corresponding to the weak, moderate, and strong turbulence, respectively. The values of C_n^2 for the weak, moderate, and strong turbulence, are chosen as 3×10^{-16}, 10^{-15}, and 5×10^{-15} $m^{-2/3}$, respectively, for an FSO link with d_i= 4 km, where λ is the optical wavelength of λ = 1550 nm and α_a = 0.43 dB/km.

III. Statistics Analysis of TAS Opportunistic Scheduling for MU-MIMO FSO System

In this section, we analyze the statistics of the MU-MIMO FSO system with the TAS opportunistic scheme. The goal of the TAS is to activate the user transmit lasers to ensure maximum irradiance at the receiver. Therefore, a feedback link and channel state information (CSI) are required. The combined irradiance over the legitimate $T \to R$ links received by R can then be expressed as follows [33]

$$I_r = \max_{m=1,\ldots,M_i}\sum_{n=1}^{N_i} I_{ir}^{mn} \tag{6}$$

According to (1), the combined received signal y_{ir} of the ith user over the $T \to R$ links can therefore be expressed as follows

$$y_{ir} = \eta G_{ir} I_r x_i + w_{ir} \tag{7}$$

where w_{ir} is the sum of w_{ir}^{mn}; and its variance is equal to $N_iN_0/2$. Thus, the combined SNR between the ith user and R can be expressed as $\gamma_r = 2(\eta G_{ir}I_r x_i)^2/N_iN_0$, and its average is given as $\bar{\gamma}_r = 2(\eta G_{ir}\mathbb{E}[I_r]x_i)^2/N_iN_0 = 2(\eta G_{ir}x_i)^2/N_iN_0$ since I_r is normalized to unity, where $\mathbb{E}[.]$ denotes the expectation operator.

Traditionally, the PDF and the CDF of the Malaga-M distribution are usually expressed by Meijer's G-function. However, the function is too complex to express the performance in closed form when applied to a MIMO FSO environment. To overcome this inconvenience, the PDF of the Malaga-M distribution is represented by a power series expansion of the modified Bessel function [50] based on the fact that the behavior of the PDF near the origin dominates the asymptotic behavior of the system performance. Based on the above, we next approximate the PDF expression of (2) as follows

$$f_{I_{ir}^{mn}}(I) \approx a_0 I^{\beta_r-1} + a_1 I^{\beta_r} \tag{8}$$

Here, we consider the first two terms of the power series expansion as

$$a_0 = \frac{A_r\sum_{j=1}^{\beta_r} a_j\Gamma(\alpha_r-\beta_r)}{\Gamma(\alpha_r)\Gamma(\beta_r)}(\alpha_r\beta_r)^{\beta_r};$$

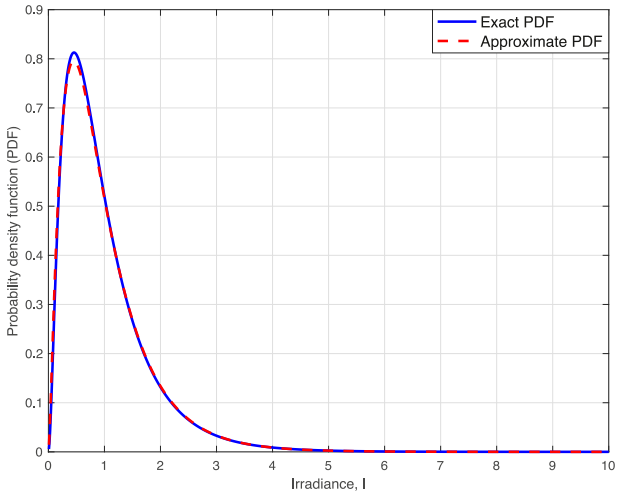

Fig. 2. Comparison of approximate and exact PDF of the considered system.

$$a_1 = \frac{A_r \sum_{j=1}^{\beta_r} a_j \Gamma(\alpha_r - \beta_r)(\alpha_r \beta_r)^{\beta_r+1}}{\Gamma(\alpha_r)\Gamma(\beta_r)(1-\alpha_r+\beta_r)} \tag{9}$$

The crucial step in our subsequent calculations is to write (8) as $f_{I_{ir}^{mn}}(I) \approx a_0 I^{\beta_r-1}(\frac{a_1}{a_0} I + 1)$, which can be further approximated by $f_{I_{ir}^{mn}}(I) \approx a_0 I^{\beta_r-1} e^{\frac{a_1}{a_0} I}$, adopting the approximation method proposed in [51]. This method approximates the exponential function near the origin by the first two terms of the Taylor series expansion so that the obtained function can be related to the gamma PDF. Replacing a_0 and a_1 by their values from (9), the PDF and CDF of the irradiance along $T \to R$ links around the origin can be advantageously approximated by

$$f_{I_r^{mn}}(x) \approx C_i \, f_M(I, \beta_r, A_i) \tag{10}$$

$$F_{I_r^{mn}}(x) \approx \frac{C_i}{\Gamma(\beta_r)} \gamma_{inc}\left(\beta_r, \frac{x}{A_i}\right) \tag{11}$$

where, $f_M(I,k,\theta) = \frac{1}{\Gamma(k)\theta^k} I^{k-1} e^{-x/\theta}$ stands for the gamma PDF with shape parameter k and scale parameter θ. In (10) and (11), $C_i = \frac{(\alpha_r-\beta_r-1)^{\beta_r}\Gamma(\alpha_r-\beta_r)}{\Gamma(\alpha_r)}$, $A_i = \frac{\alpha_r-\beta_r-1}{\alpha_r\beta_r}$, are two constants related to the α_r, and β_r parameters of the legitimate $T \to R$ links, $\gamma_{inc}(a,x) = \int_0^x t^{a-1} \exp(-t) dt$ is the lower incomplete gamma function [32]. A plot of the exact PDF of (2) and the derived approximate PDF of (8) is shown in Fig. 2 for $C_n^2 = 3 \times 10^{-16}$. From Fig. 2, it can be seen that a closed match between the exact PDF and the approximate PDF in Fig. 2 can be observed, which shows the correctness of our derived results.

Based on the theory of order statistics [52], the CDF of $T \to R$ links combined irradiance I_r can be approximated as follows

$$F_{\max\limits_{m=1,\ldots,M_i} \sum\limits_{n=1}^{N_i} I_r^{mn}}(x) \approx \left[\frac{C^{N_i}}{\Gamma(N_i\beta_r)} \gamma_{inc}\left(N_i\beta_r, \frac{x}{A_i}\right)\right]^{M_i} \tag{12}$$

According to the TAS, R is assumed to select the kth best user per time slot, assuming it knows all the information about the channel state. Such a TAS scheme was originally applied in multiuser RF systems to provide a multiuser scheduling solution with low complexity [53]. The SNRs of the ith users γ_i are arranged in descending order of feedback value, $\gamma_1 \geq \gamma_2 \geq \cdots \geq \gamma_K$, and γ_k denotes the kth best user SNR. In this case, the TAS-based SNR is given by [54, Eq. (7)]

$$\gamma_k = \bar{\gamma}_r \left(\Im \max_{i=1,\ldots,K} I_{r_i}\right)^s \tag{13}$$

where $\Im$ represents the impairments due to the pointing errors, which are assumed to be the same for all $T \to R$ links, s is the parameter defining the type of detection technique in the FSO receiver, i.e., $s = 1$ represents heterodyne detection, and $s = 2$ represents intensity modulation/direct detection (IM/DD). To simplify the calculation, we assume that each link has the same number of transmit apertures ($M_i = M$) and receive apertures ($N_i = N$), for $i = \{1, \cdots, K\}$, and also has the same average link distance $\bar{d}$. Based on the assumptions, the SNRs are independent and identical distributions (i.i.d). Based on this assumption and using [55, Eq. (6)], the CDF of the $T \to R$ links in terms of the kth best user's SNR can be reduced to

$$F_{\gamma_k}(x) = \sum_{i=K-k+1}^{K} \binom{K}{i} [F_r(x)]^i [1 - F_r(x)]^{K-i} \tag{14}$$

where $F_r(x)$ is the CDF of legitimate $T \to R$ links defined by (12). Applying (12) to (14), the CDF of the MIMO FSO links concerning the SNR of the kth best user is obtained as follows

$$F_{\gamma_k}(x) = \sum_{i=K-k+1}^{K} \sum_{j=0}^{K-i} \binom{K}{i} \binom{K-i}{j} (-1)^j \times \left[\frac{C^N}{\Gamma(N\beta_r)} \gamma_{inc}\left(N\beta_r, \frac{x}{A}\right)\right]^L \tag{15}$$

where $L = M(i+j)$. Replacing the lower incomplete Gamma function in (15) by its series expansion $\gamma_{inc}(\mathrm{n}, \mathrm{z}) = (n-1)![1 - e^{-z} \sum_{m=0}^{n-1} \frac{z^m}{m1}]$ [56, Eq. (8.352.6)] and applying the multinomial expansion, the CDF of the $T \to R$ links with respect to γ_k can be represented as follows

$$\begin{aligned} F_{\gamma_k}(\gamma) &= \mathbb{E}_\Im \left\{ \left[F_{\gamma_k}\left(\frac{1}{\Im}\left(\frac{\gamma}{\bar{\gamma}_r}\right)^{\frac{1}{s}}\right)\right]^L \right\} \\ &= \Psi_1 \sum_{l=1}^{L} \sum_{\Upsilon} \tau_t \mathbb{E}_\Im \\ &\quad \times \left\{ e^{(-lB_r\left(\frac{\gamma}{\bar{\gamma}_r}\right)^{\frac{1}{s}}/\Im A)} \left(\frac{\gamma}{\bar{\gamma}_r}\right)^{\frac{\delta_l}{s}} \left(\frac{1}{\Im A}\right)^{\delta_l} \right\} \end{aligned} \tag{16}$$

where $\Psi_1 = \sum_{i=K-k+1}^{K} \sum_{j=0}^{K-i} \binom{K}{i}\binom{K-i}{j} (-1)^j \frac{C^{LN}}{\Gamma(N\beta_r)^L}$, $\delta_l = \sum_{l=0}^{N\beta_r-1} l t_{l+1}$, $\sum_{\Upsilon} = \sum_{\Upsilon_{l,N\beta_r}} \sum_{\Upsilon_{l,t_1}} \sum_{\Upsilon_{l,t_2}} \cdots \sum_{\Upsilon_{l,t_l}}$, $\Upsilon_{z,l} = \{(z_1, .., z_l) : z_i \geq 0, \sum_{i=1}^{l} z_i = z\}$, $B_r = \frac{\alpha_r\beta_r}{(g\beta_r+\Omega)^r}$, while $\tau_t = \prod_{r=1}^{N\beta_r} \frac{\Gamma(N\beta_r-1)^{Lt_{Pr}} \binom{L}{t} (-1)^{t+1} t!}{\prod_{p=1}^{t}(t_p-1)!}$.

Recall the PDF of generalized nonzero boresight pointing errors, which can be accurately approximated by a modified Rayleigh distribution [57] as follows

$$f_\Xi(x) \simeq \frac{\varphi_r^2}{(\mathrm{A}_O G_f)^{\varphi_r^2}} x^{\varphi_r^2-1}, \; 0 \leq x \leq \mathrm{A}_O G_f \tag{17}$$

where $\varphi_r = \frac{w_{L(eq)}}{2\sigma_{mod}}$ is the ratio of the equivalent beam radius, $w_{L_{(eq)}}$, and the standard deviation (jitter) at the receiver plane, $(2\sigma_{mod})$, $\varphi_x = \frac{w_{L(eq)}}{2\sigma_x}$, $\varphi_y = \frac{w_{L(eq)}}{2\sigma_y}$, $\mathrm{A}_O = [erf(v)]^2$, $erf(\cdot)$ denotes the error function, $v = \frac{\sqrt{\pi}a}{\sqrt{2}w_{L(eq)}}$, a is the aperture radius of the photodetector, and $G_f = exp(\frac{1}{\varphi^2} - \frac{1}{2\varphi_x^2} - \frac{1}{2\varphi_y^2} - \frac{\mu_x^2}{2\sigma_x^2\varphi_x^2} - \frac{\mu_y^2}{2\sigma_y^2\varphi_y^2})$.

From (16), the CDF of TAS-based SNR, taking into account the effect of the generalized pointing errors, is given as

$$F_{\gamma_k}(\gamma) = \frac{\Psi_1\varphi_r^2\sum_{l=1}^{L}\sum_{\Upsilon}\tau_t}{A_0^{\varphi_r^2}}\left(\frac{\gamma}{\bar{\gamma}_r}\right)^{\frac{\delta_l}{s}} \int_0^{A_0} x^{\varphi_r^2-\delta_l-1} G_{10}^{01}\left[\frac{lB_r x}{A}\left(\frac{\gamma}{\bar{\gamma}_r}\right)^{\frac{1}{s}}\middle|\begin{matrix}1\\0\end{matrix}\right]dx, \quad (18)$$

where (18) follows from the substitution of the exponential function with [58, Eq. (8.4.3.1)]. Applying [59, Eq. (07.34.21.0084.01)] to (18) yields

$$F_{\gamma_k}(\gamma) = \frac{\Psi_1\varphi_r^2\sum_{l=1}^{L}\sum_{\Upsilon}\tau_t}{2\pi A_0^{\varphi_r^2}}\left(\frac{\gamma}{\bar{\gamma}_r}\right)^{\frac{\delta_l}{s}} G_{21}^{02} \times\left[\frac{lB_r}{A}\left(\frac{\gamma}{\bar{\gamma}_r}\right)^{\frac{1}{s}}\middle|\begin{matrix}1-\varphi_r^2+\delta_l, 1\\ 1-\varphi_r^2-\delta_l\end{matrix}\right] \quad (19)$$

IV. Performance Analysis

In this section, we evaluate the outage probability, and the average BER of the considered system.

A. Outage Probability

The outage probability is defined as the probability that the SNR at the receiver falls below a given outage threshold γ_{th}, i.e., $P_{\text{out}} = P_r[\gamma_r \leq \gamma_{th}]$, where $P_r[.]$ denotes the probability operation, γ_r is the SNR at R, and $\gamma_{th} = 2^{\mathcal{R}} - 1$, where $\mathcal{R}$ denotes the target data rate. Thus, the outage probability can be obtained by replacing γ with γ_{th} in the CDF expressions (19) as follows

$$P_{\text{out}} = \frac{\Psi_1\varphi_r^2\sum_{l=1}^{L}\sum_{\Upsilon}\tau_t}{2\pi A_0^{\varphi_r^2}}\left(\frac{\gamma_{th}}{\bar{\gamma}_r}\right)^{\frac{\delta_l}{s}} G_{21}^{02} \times\left[\frac{lB_r}{A}\left(\frac{\gamma_{th}}{\bar{\gamma}_r}\right)^{\frac{1}{s}}\middle|\begin{matrix}\Delta_1\\ \Delta_2\end{matrix}\right] \quad (20)$$

where $\Delta_1 = 1-\varphi_r^2+\delta_l, 1$ and $\Delta_2 = 1-\varphi_r^2-\delta_l$.

Eq. (20) can be further expressed in terms of the H-function [59, Eq. (07.34.26.0008.01)] as follows

$$P_{\text{out}} = \frac{\Psi_1\varphi_r^2\sum_{l=1}^{L}\sum_{\Upsilon}\tau_t}{2\pi A_0^{\varphi_r^2}}\left(\frac{\gamma_{th}}{\bar{\gamma}_r}\right)^{\frac{\delta_l}{s}} H_{21}^{02} \times\left[\frac{lB_r}{A}\left(\frac{\gamma_{th}}{\bar{\gamma}_r}\right)^{\frac{1}{s}}\middle|\begin{matrix}(\zeta_1,\ \zeta_2)\\ (\phi_1,\ \phi_2)\end{matrix}\right] \quad (21)$$

where $(\zeta_1,\ \zeta_2) = (1-\varphi_r^2+\delta_l,\ s)$, $(1,\ s)$ and $(\phi_1,\ \phi_2) = (1-\varphi_r^2-\delta_l,\ s)$.

To gain further insight into the high SNR regime, we analyzed the asymptotic behavior of (21) and presented it in an easy-to-follow form with reasonable accuracy. At high SNR values, the outage probability of the FSO system can be expressed as $P_{\text{out}}^{Asy} \approx (\mathbb{G}_c\ SNR)^{-\mathbb{G}_d}$, where $\mathbb{G}_c$ and $\mathbb{G}_d$ denote the system's coding gain and diversity order, respectively. For this purpose, we invoke asymptotic expansions of the Fox-H function [60, Theorems 1.7 and 1.11]. Based on (21), the asymptotic behavior of the outage probability for the $\bar{\gamma}_r \to \infty$ is derived as

$$P_{\text{out}}^{Asy} \approx \frac{\Psi_1\varphi_r^2\sum_{l=1}^{L}\sum_{\Upsilon}\tau_t}{2\pi A_0^{\varphi_r^2}}\left(\frac{\gamma_{th}}{\bar{\gamma}_r}\right)^{\frac{\delta_l}{s}}\sum_{t=1}^{2}\frac{1}{\zeta_{2t}} \times\frac{\prod_{\substack{s=1\\ s\neq t}}^{2}\Gamma\left(1-\zeta_{1s}-\zeta_{1t}\frac{\zeta_{2s}}{\zeta_{2t}}\right)}{\Gamma\left(1-\zeta_{1s}-\phi_{1t}\frac{\zeta_{2s}}{\phi_{2t}}\right)}\left(\frac{lB_r\gamma_{th}}{A\bar{\gamma}_r}\right)^{\left(\frac{\phi_{1t}}{\phi_{2t}}+1\right)} \quad (22)$$

The diversity gain of the considered system over atmospheric turbulence conditions is inferred as $\mathbb{G}_d = \min\{\frac{\varphi_r^2}{s}, \frac{\alpha_r}{s}, \frac{\beta_r}{s}\}$.

B. Average Bit Error Probability

Substituting (19) into [61, Eq. (12)] and utilizing [56, Eq. (7.813.1)] and [59, Eq. (07.34.26.0008.01)], the average BER P_b can be expressed in terms of the CDF of γ_k as

$$P_b = \Psi_2\left(\frac{1}{\bar{\gamma}_r}\right)^{\frac{\delta_l}{s}} H_{31}^{03}\left[\frac{dlB_r}{A}\left(\frac{1}{\bar{\gamma}_r}\right)^{\frac{1}{s}}\middle|\begin{matrix}(\aleph_1,\ \aleph_2)\\ (\mathfrak{U}_1,\ \mathfrak{U}_2)\end{matrix}\right] \quad (23)$$

where $\Psi_2 = \frac{\Psi_1\varphi_r^2\sum_{l=1}^{L}\sum_{\Upsilon}\tau_t\ d^{-c-\frac{\delta_l}{s}}}{4\pi A_0^{\varphi_r^2}\Gamma(c)}$, $(\aleph_1,\ \aleph_2) = (1-c-\frac{\delta_l}{s}, s)$, $(1-\varphi_r^2+\delta_l,\ s)$, $(1,\ s)$ and $(\mathfrak{U}_1,\ \mathfrak{U}_2) = (1-\varphi_r^2-\delta_l,\ s)$, c and d are modulation specific parameters. Similar to the P_{out}, the average BER can be expressed asymptotically, at high SNR, as

$$P_b^{Asy} \approx \Psi_2\left(\frac{1}{\bar{\gamma}_r}\right)^{\frac{\delta_l}{s}}\sum_{z=1}^{3}\frac{1}{\aleph_{2z}} \times\frac{\prod_{\substack{v=1\\ v\neq z}}^{3}\Gamma\left(1-\aleph_{1v}-\aleph_{1z}\frac{\aleph_{2v}}{\aleph_{2z}}\right)}{\Gamma\left(1-\aleph_{1v}-\mathfrak{U}_{1z}\frac{\aleph_{2v}}{\mathfrak{U}_{2z}}\right)}\left(\frac{dlB_r}{A\bar{\gamma}_r}\right)^{\left(\frac{\mathfrak{U}_{1z}}{\mathfrak{U}_{2z}}+1\right)} \quad (24)$$

V. Security Analysis

In this section, we analyze the secrecy performance of the MU-MIMO FSO system in the presence of a single eavesdropper E equipped with a P aperture. When T sends its signals to R, they can be intercepted by E, as shown in Fig. 1. It is assumed that E is in the receiving plane of R, and thus, it can also overhear the transmission from T. Therefore, E can combine its signals received from T to obtain an enhanced signal version using equal gain combining (EGC). Typically, EGC is

usually able to achieve better combining performance due to its low complexity implementation compared to other combining techniques. Therefore, we consider using EGC at E to maximize its ability to interpret the transmitted message. Thus, the received signal at E is given by

$$y_{te} = \frac{\eta x_k}{MP} \sum_{i}^{M} \sum_{t=1}^{P} I_{ite} + v_e \tag{25}$$

where I_{ite} is the irradiation coefficient of the interception link between the ith user of T and the tth interception aperture of E, and v_e is an AWGN sample at E. Since E applies the EGC scheme, the combined SNR observed at E can be expressed as [62]

$$\gamma_{ie} = \frac{\eta^2}{MPN_o} \sum_{t=1}^{P} I_{ite}^2 \tag{26}$$

For this case, the PDF of the $T \to E$ links, which follows a Malaga-M distribution in the form of the Meijer G-function, is given as follows [63]

$$f_{\gamma_{ie}}(\gamma) = \frac{\varphi_e^2 A_e}{4\gamma^{\frac{1}{s}}} \sum_{j=1}^{\beta_e} a_{je}\, G_{1,3}^{3,0}\left(B_e \left(\frac{\gamma}{\bar{\gamma}_e}\right)^{\frac{1}{s}} \middle| \begin{matrix} \varphi_e^2+1 \\ \varphi_e^2, \alpha_e, j \end{matrix} \right) \tag{27}$$

where α_e and β_e are the new shaping parameters, defined as $\alpha_e = P\alpha_E$ and $\beta_e = P\beta_E$, α_E and β_E are the two parameters related to atmospheric conditions via the $T \to E$ links, φ_e is the ratio of the equivalent beam radius, and the standard deviation in the E-plane, $\bar{\gamma}_e = \frac{\eta^2 x_k^2}{MPN_o}$. The CDF expression is obtained using (27) and [59, Eq. (07.34.21.0084.01)], which is given by

$$F_{\gamma_{ie}}(\gamma) = \frac{\varphi_e^2 A_e}{2} \sum_{j=1}^{\beta_e} a_{je}\, G_{24}^{31}\left(B_e \left(\frac{\gamma}{\bar{\gamma}_e}\right)^{\frac{1}{s}} \middle| \begin{matrix} 1,\ \varphi_e^2+1 \\ \varphi_e^2, \alpha_e, j, 0 \end{matrix} \right) \tag{28}$$

To facilitate dealing with the complexity of the MIMO FSO channel of $T \to E$ links with the EGC diversity technique in E, we adopt an alternative representation of the CDF of the Malaga-M fading channels. Hence, a simplified expression of (28) is obtained by using [59, Eq. (07.32.02.0001.01)] and [59, Eq. (06.10.02.0001.01)], as

$$F_{\gamma_{ie}}(\gamma) = \frac{\varphi_e^2 A_e}{2} \sum_{j=1}^{\beta_e} a_{j,e} \pi^2 \left[\sum_{k=0}^{\infty} \frac{X_{1,k}^i}{\Omega_{1,k}^i} \gamma^{\Omega_{1,k}^i} + \sum_{p=0}^{\infty} \frac{X_{2,p}^i}{\Omega_{2,p}} \gamma^{\Omega_{2,p}} + \sum_{q=0}^{\infty} \frac{X_{3,q}^i}{\Omega_{3,q}} \gamma^{\Omega_{3,q}} \right] \tag{29}$$

where $X_{1,k}^i, X_{2,p}^i, X_{3,q}^i, \Omega_{1,k}^i, \Omega_{2,p}$, and $\Omega_{3,q}$ are given in Table I.

The above series representation of the CDF of Malaga-M distribution of (29), contains three power series. Each series contains summation terms with only exponents of X. Therefore, it is easy to compute an integral containing the proposed series representation compared to a complicated function-based representation in (28). By applying the ratio test for each power series in (29), it can be shown that the above series representation contains converging power series with an infinite radius of convergence. Using the Cauchy ratio test to check convergence, the series $\sum X_k$ is absolutely convergent if [64, Eq. (10)] as $\lim_{k\to\infty} |\frac{X_{k+1}}{X_k}| < 0$. The radius of convergence of the first subseries in (29) $\frac{X_{1,k}^i}{\Omega_{1,k}^i}$ is given by

$$r_1 = \lim_{k\to\infty} \left| \frac{X_{1,k+1}^i / \Omega_{1,k+1}^i}{X_{1,k}^i / \Omega_{1,k}^i} \right|$$
$$r_1 = \lim_{k\to\infty} \left| \frac{k v_i}{(k+1)\,(k-\alpha_e-\varphi_e^2+1)\,(k-j-\varphi_e^2+1)} \right| \tag{30}$$

It can be seen from (30) that the order of k in the denominator is higher than the numerator. So, applying limit $k \to \infty$ in (30) gives 0; hence, r_1 is absolutely convergent [64]. In a similar manner, the series in $\frac{X_{2,p}^i}{\Omega_{2,p}}$ and $\frac{X_{3,q}^i}{\Omega_{3,q}}$ can be shown to be convergent.

Hence, the CDF of the $T \to E$ links with M and P apertures in T and E, respectively, is given by [63]

$$F_{\gamma_e}(\gamma) = \prod_{i=1}^{\mathrm{M}} \prod_{t=1}^{\mathrm{P}} F_{\gamma_{ie}}(\gamma), \tag{31}$$

where $F_{\gamma_{ie}}(\gamma)$ is given by (29). Hence, the PDF of the $T \to E$ links with respect to γ_e can be obtained as

$$f_{\gamma_e}(\gamma) = MP f_{\gamma_{ie}}(\gamma) \left[F_{\gamma_e}(\gamma)\right]^{MP-1}, \tag{32}$$

where $f_{\gamma_{ie}}(\gamma)$ is given by (27). Substituting (27) and (29) into (32) and applying the binomial theorem yields the expression for $f_{\gamma_e}(\gamma)$ shown in the following,

$$f_{\gamma_e}(\gamma) = \frac{MP\varphi_e^2 A_e}{4} \sum_{j=1}^{\beta_e} a_{je} \left(\frac{\varphi_e^2 A_e \pi^2}{4}\right)^{MP-1} \times \left(\sum_{j=1}^{\beta_e} a_{je}\right)^{MP-1} \Lambda_e \gamma^{\frac{1+MP+\delta_L}{s}+\tau-1} G_{13}^{30} \times \left(B_e \left(\frac{\gamma}{\bar{\gamma}_e}\right)^{\frac{1}{s}} \middle| \begin{matrix} \varphi_e^2+1 \\ \varphi_e^2, \alpha_e, j \end{matrix} \right) \tag{33}$$

where

$$\Lambda_e = \sum_{k_e=0}^{MP-1} \binom{MP-1}{k_e} \sum_{r=0}^{MP-1-k_e} \binom{MP-1-k_e}{r} \prod_{j=1}^{MP-1} \left(\sum_{k=0}^{\infty} \frac{X_{1,k}^i}{\Omega_{1,k}^i}\right) \prod_{p=1}^{MP-1-k_e} \left(\sum_{p=0}^{\infty} \frac{X_{2,p}^i}{\Omega_{2,p}}\right) \prod_{q=1}^{MP-1-k_e-r} \left(\sum_{q=0}^{\infty} \frac{X_{3,q}^i}{\Omega_{3,q}}\right) \tag{34}$$

where τ is given in Table I.

A. Intercept Probability Based on TAS Opportunistic Scheme

Intercept probability is an important metric that provides further insight into the secrecy performance of a communication system. It is defined as the probability that the capacity of the

main link is less than that of the wiretap channel. Mathematically, the intercept probability is formulated as follows [65]

$$\begin{aligned} P_{\text{int}} &= P_r\ (C_r < C_e) \\ &= \int_0^{\infty} \int_0^{\gamma_e} f_{\gamma_r}(\gamma_r)\ f_{\gamma_e}(\gamma_e)\ d\gamma_r d\gamma_e \\ &= \int_0^{\infty} F_{\gamma_r}(\gamma_r)\ f_{\gamma_e}(\gamma_e)\, d\gamma_e \end{aligned} \tag{35}$$

where C_r denotes the channel capacity of the legitimate $T \to R$ links

$$C_r = \log(1+\gamma_r) \tag{36}$$

and C_e is the channel capacity of the eavesdropping $T \to E$ links

$$C_e = \log(1+\gamma_e) \tag{37}$$

where f_{γ_e} is the PDF of the wiretap links obtained from (33). The integration of (35) can be calculated by substituting (18) and (33) into (35) and using [59, Eq. (07.34.26.0008.01)] to convert the Meijer G-function terms in (18) and (31) into the Fox H-function, then by using [60, Eq. (1.8.5)], we have

$$\begin{aligned} P_{\text{int}}^{TAS} = \Psi_3 \left(\frac{B_e}{\bar{\gamma}_e}\right)^{-\left(\frac{1+MP+2\delta_l}{s}+\tau\right)} H_{52}^{05} \\ \times \left[\frac{lB_r\bar{\gamma}_e}{AB_e\bar{\gamma}_r}\,\middle|\, \begin{matrix}(\psi_1,\ \psi_2)\\ (\forall_1,\ \forall_2)\end{matrix}\right] \end{aligned} \tag{38}$$

where $(\psi_1,\ \psi_2) = (1+\varphi_r^2+\delta_l, s), (1,s), (-\varphi_e^2-1-MP-2\delta_l-s\tau, s), (1-\alpha_e-1-MP-2\delta_l-s\tau, s), (1-j-1-MP-2\delta_l-s\tau, s)$, $(\forall_1,\ \forall_2) = (1-\varphi_r^2-\delta_l, s)$, $(-\varphi_e^2, 1-MP-2\delta_l-s\tau, s)$, and

$$\begin{aligned} \Psi_3 = \frac{\Psi_1 \varphi_r^2 s^2 \sum_{l=1}^{L}\sum_{\Upsilon}\tau_t\, MP\varphi_e^2 A_e \left(\sum_{j=1}^{\beta_e} a_{je}\right)^{MP-1}}{4(2\pi)^{s-1} A_0^{\varphi_r^2} \bar{\gamma}_r^{\frac{\delta_l}{s}}} \\ \times \sum_{j=1}^{\beta_e} a_{j,e} \left(\frac{\varphi_e^2 A_e \pi^2}{4\gamma}\right)^{MP-1} \Lambda_e \end{aligned} \tag{39}$$

To analyze the asymptotic behavior of the intercept probability in the range of high SNR values, we first recall [60, Eq. (1.8.15)] and [60, Eq. (1.8.5)] and further perform some algebraic manipulations as follows

$$\begin{aligned} P_{\text{int}}^{Asy} = \Psi_3 \left(\frac{B_e}{\bar{\gamma}_e}\right)^{-\left(\frac{1+MP+2\delta_l}{s}+\tau\right)} \sum_{t=1}^{5} \frac{1}{\psi_{2t}} \\ \times \frac{\prod_{\substack{s=1\\ s\neq t}}^{5} \Gamma\left(1-\psi_{1s}-\psi_{1t}\frac{\psi_{2s}}{\psi_{2t}}\right)}{\prod_{t=1}^{2}\Gamma\left(1-\forall_{1s}-\psi_{1t}\frac{\forall_{2s}}{\psi_{2t}}\right)} \left(\frac{AB_e\bar{\gamma}_r}{lB_r\bar{\gamma}_e}\right)^{\frac{1-\psi_{1t}}{\psi_{2t}}+1} \end{aligned} \tag{40}$$

VI. Security-Reliability Trade-Off

In this section, we develop an expression of the SRT for the MU-MIMO FSO system that considers the system's predetermined outage threshold. The outage threshold corresponds to the threshold SNR γ_{th} below which detection is very unlikely at the given data rate. An interception occurs when the eavesdropper detects the signal with an SNR above this threshold. Meanwhile, the SRT can be represented as follows [6]

$$\begin{aligned} P_{int,th} &= P_r\ (\gamma_r \le \gamma_e, \gamma_e > \gamma_{th}) \\ &= P_r\ (\gamma_r \le \gamma_e)\, P_r\,(\gamma_e > \gamma_{th}) \end{aligned} \tag{41}$$

where $P_r(\gamma_r \le \gamma_e)$ and $P_r(\gamma_e > \gamma_{th})$ represent the intercept probability and the outage probability of the legitimate $T \to R$ and $T \to E$ links, respectively. Eq. (41) can be rewritten as

$$\begin{aligned} P_{int,th} &= P_r\ (\gamma_k \le \gamma_e, \gamma_e > \gamma_{th}) \\ &= P_{\text{int}}^{TAS} \times F_{\gamma_e}(\gamma_{th}). \end{aligned} \tag{42}$$

Thus, by substituting (29) and (38) in (42), we have

$$\begin{aligned} P_{int,th} = \frac{\Psi_3\Lambda_e}{s}\left(\frac{\varphi_e^2 A_e \pi^2}{4}\right)^{MP-1}\left(\sum_{j=1}^{\beta_e} a_{je}\right)^{MP-1} \\ \left(\frac{B_e}{\bar{\gamma}_e}\right)^{-\left(\frac{1+MP+2\delta_l}{s}+\tau\right)} \gamma_{th}^{\frac{1+MP+\delta_l}{s}+\tau} H_{52}^{05}\left[\frac{lB_r\bar{\gamma}_e}{AB_e\bar{\gamma}_r}\,\middle|\, \begin{matrix}(\psi_1,\ \psi_2)\\ (\forall_1,\ \forall_2)\end{matrix}\right] \end{aligned} \tag{43}$$

The asymptotic behavior of the $P_{int,th}$ is derived for the $\bar{\gamma}_r \to \infty$ as

$$\begin{aligned} P_{int,th}^{Asy} = \Psi_3 \left(\frac{\varphi_e^2 A_e \pi^2}{4}\right)^{MP-1}\left(\frac{B_e}{\bar{\gamma}_e}\right)^{-\left(\frac{1+MP+2\delta_l}{s}+\tau\right)} \\ \times \left(\sum_{j=1}^{\beta_e} a_{je}\right)^{MP-1} \Lambda_e \gamma_{th}^{\frac{1+MP+\delta_l}{s}+\tau} \sum_{t=1}^{5}\frac{1}{\psi_{2t}} \\ \times \frac{\prod_{\substack{s=1\\ s\neq t}}^{5}\Gamma\left(1-\psi_{1s}-\psi_{1t}\frac{\psi_{2s}}{\psi_{2t}}\right)}{\prod_{t=1}^{2}\Gamma\left(1-\forall_{1s}-\psi_{1t}\frac{\forall_{2s}}{\psi_{2t}}\right)} \\ \times \left(\frac{AB_e\bar{\gamma}_r}{lB_r\bar{\gamma}_e}\right)^{\frac{1-\psi_{1t}}{\psi_{2t}}+1} \end{aligned} \tag{44}$$

VII. Numerical Results

Selected simulation results of the MU-MIMO FSO system considering eavesdropping situations are provided and analyzed in this section using the above analytical expressions. We investigate the effects of atmospheric turbulence, generalized pointing errors, the number of users, and the power received from the eavesdropper on the outage probability, intercept probability, and SRT performance of the system under consideration. For simplicity, we assume independent, identically distributed main and wiretap channels. Moreover, the average optical power of the FSO links is assumed to be $b_o = 0.25$, $\Omega = 0.5$, and $\rho = 0.95$. The graphs were generated in MATLAB using analytical equations and Monte Carlo simulations with 10^6 channel realizations to confirm the accuracy and usefulness of the proposed approximation. Unless stated otherwise, the considered system and channel simulation parameters are listed in Table II.

TABLE II
SIMULATION PARAMETERS

AWGN variance	N_o	10^{-14} A^2/GHz
Link distance	d_i	4000 m
Transmission rate	$\mathcal{R}$	1 bit/s/Hz
Optical wavelength	λ	1550 nm
Normalized beam-width	$w_{L_{(eq)}} / a,$	10 cm
Normalized Horizontal and vertical displacement	$\{\mu_x / a, \mu_y / a\}$	$\{1, 2\}$ cm
Aperture radius	a	5 cm
Normalized standard deviation	$(\sigma_x/a\,, \sigma_y/a)$	$\{(9,7), (2,1)\}$.
Atmospheric attenuation	α_a	0.43 dB/km
Weak, moderate, and strong refractive index structure	C_n^2	3×10^{-16}, 10^{-15}, 5×10^{-15} m$^{-2/3}$

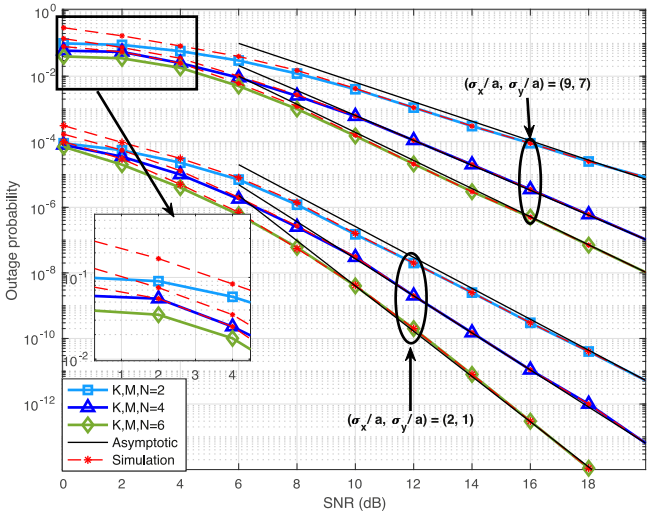

Fig. 3. Outage probability versus $\bar{\gamma}_r$ for selected values of K, M, and N.

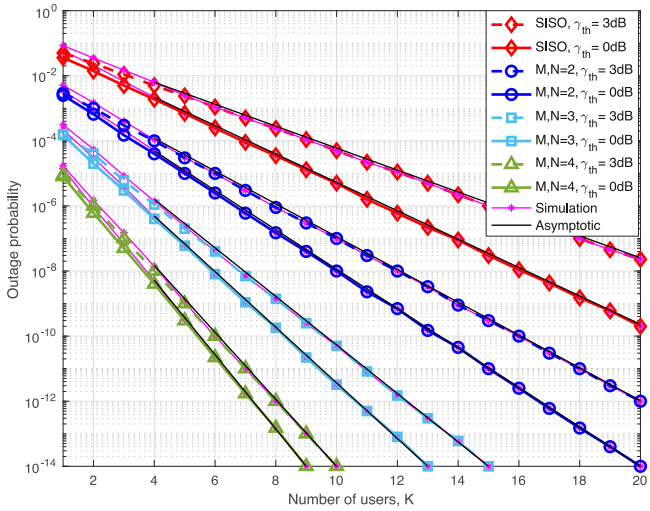

Fig. 4. Outage probability versus K for different numbers of M, and N.

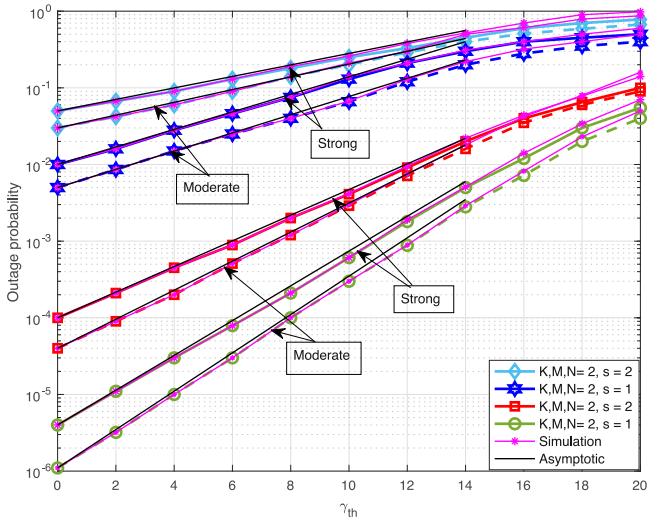

Fig. 5. Outage probability versus γ_{th} for the different K, M, and N numbers.

First, results corresponding to the outage performance analysis described in Section IV are shown in Fig. 3 for moderate turbulence as a function of average electrical SNR, $\bar{\gamma}_r$, with γ_{th} = 5 dB. In Fig. 3, two normalized jitter values $(\sigma_x/a,\ \sigma_y/a) = \{(2, 1), (9, 7)\}$ are considered to carefully analyze how $T \rightarrow R$ links are affected by generalized pointing errors. As seen from Fig. 3, a more significant number of users, K, leads to a lower outage probability, indicating a linear relationship between the diversity order and K. Moreover, the best performance is obtained when the jitter value is small $(\sigma_x/a,\ \sigma_y/a) = (2, 1)$, since the photodetector is better positioned in this case. Moreover, the analytical curves agree with the simulation curves in the high SNR region, proving the derived formulas' correctness. However, the analytical results in the low SNR region deviate from the simulation results as clearly shown in Fig. 3. This is due to the approximation method in (8), where only the first two terms in the power series expansion of the modified Bessel function are considered to simplify the MIMO Malaga-M distribution.

Fig. 4 shows the outage probability as a function of K for selected values of γ_{th} with $\bar{\gamma}_r = 5$ dB, $(\sigma_x/a,\ \sigma_y/a) = (9, 7)$, and moderate atmospheric turbulence. Fig. 4 shows that the values of outage probability decrease linearly as the number of users increases, implying that the order of diversity has a linear relationship with K. Moreover, the results show that a higher number of apertures in T and R leads to significantly improved performance. This is because the diversity order of the system increases as the number of K, M and N increases. Compared to the system performance at a low value of γ_{th}, the negative effect of a higher value of γ_{th} on the system's outage probability is easily seen.

Next, we discuss how the threshold SNR affects the MU-MIMO FSO system's reliability. Fig. 5 shows the system's outage probability as a function of the threshold SNR, γ_{th}, for different atmospheric turbulence conditions. The results show that the increase of γ_{th} and the strength of atmospheric turbulence significantly deteriorates the outage performance for both detection schemes of R. The results also show that the system's performance decreases faster as the number of M

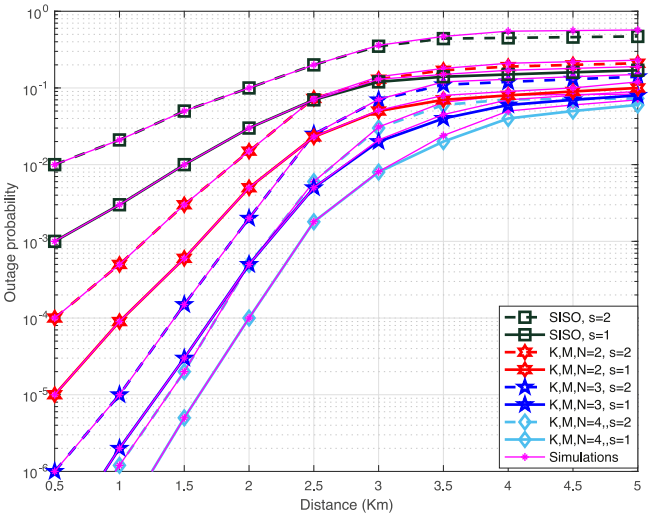

Fig. 6. Outage probability versus the FSO link's distance for various K, M, and N values.

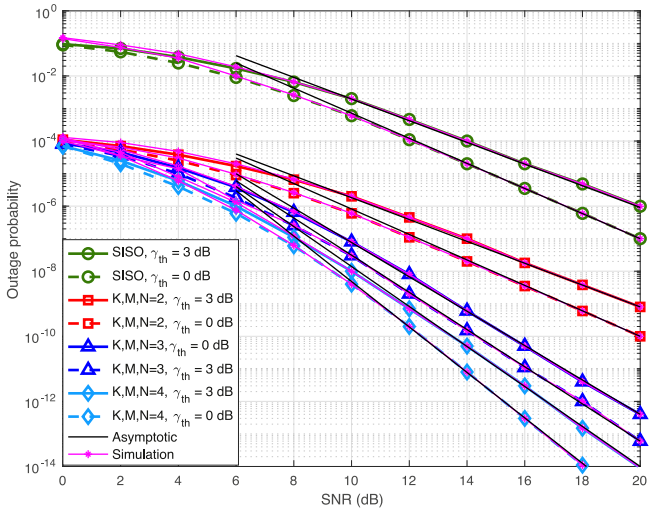

Fig. 7. Outage probability versus $\bar{\gamma}_r$ for various values of K, M, and N and selected values of γ_{th}.

and N decreases; in particular, the system achieves worst with $K, M,\ N = 2$. Moreover, the heterodyne detection outperforms the IM/DD detection for all values of N, as shown in Fig. 5.

Next, we investigate the transmission distance of the MU-MIMO FSO system by plotting the outage performance as a function of the average distance between T and R, $\bar{d}$, for different numbers of K, M, N as shown in Fig. 6. In this case, $\bar{\gamma}_r = 5$ dB, $(\sigma_x/a,\ \sigma_y/a) = (9,\ 7)$, and strong atmospheric turbulence. The results show that the outage probability increases with the length of the link, regardless of the number of K, M, or N, since the power received by R decreases for the most extended transmission distances. This phenomenon also illustrates how the scintillation index approaches saturation as the length of the link or the strength of the turbulence increases. One possible explanation is that the direct transmission component, which dominates FSO transmission, is affected by atmospheric turbulence when the selected user is far from the transmitter. In addition, the results show that heterodyne detection performs better than the IM/DD scheme at all transmission distances. While the outage probability of the SISO system increases dramatically with increasing link length, the P_{out} of the MU-MIMO FSO system is much less extreme.

Fig. 7 shows the outage performance as a function of the average SNR of the MU-MIMO and SISO FSO systems with selected values of γ_{th}. In this case, the atmospheric turbulence is assumed to be strong with $(\sigma_x/a,\ \sigma_y/a) = (9,\ 7)$. As can be seen, the P_{out} values considering both γ_{th} values decrease rapidly with increasing SNR. Moreover, the results demonstrate that the P_{out} value is enhanced with a more significant number of K, M, N compared to the SISO case. Additionally, when γ_{th} is 0 dB, the FSO system achieves the lowest P_{out}. The Monte Carlo simulations and the asymptotic results agree well with the exact results and show the accuracy of the obtained expressions at high SNR values, as shown in this figure.

Regarding the average BER analysis, we will highlight the effect of the receiver aperture's size in combination with the

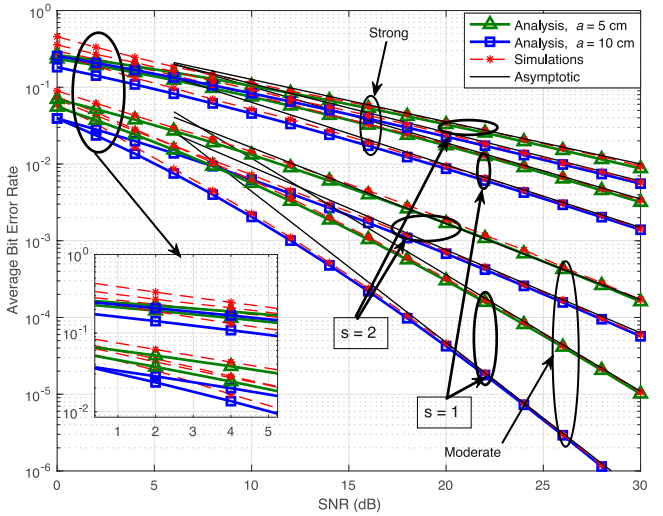

Fig. 8. Average BER versus $\bar{\gamma}_r$ for selected values of a.

atmospheric turbulence conditions on system performance as shown in Fig. 8. In this case, we consider $K, M, N = 2$ and an ignorant misalignments effect. It is clear from this figure that decreasing turbulence conditions (i.e., moderate turbulence conditions) leads to better BER performance regardless of the receiver aperture size and type of detection scheme in R. However, for a larger aperture's size of the receiver (i.e., $a = 10$ cm) a lower BER was achieved. This is because the variations in intensity at R result in a variance in received power that depends on the size of the receiver aperture. Increasing the receiver aperture size decreases the power variance and improves the bit error rate. Where the receiver aperture must be large enough to collect sufficient power to reduce scintillation effects at a given range, but also small enough to be a practical size for cost-effectiveness. In addition, it can be noticed that the degradation of the system performance due to strong turbulence is greater when IM/DD detection is employed. For instance, under moderate turbulence

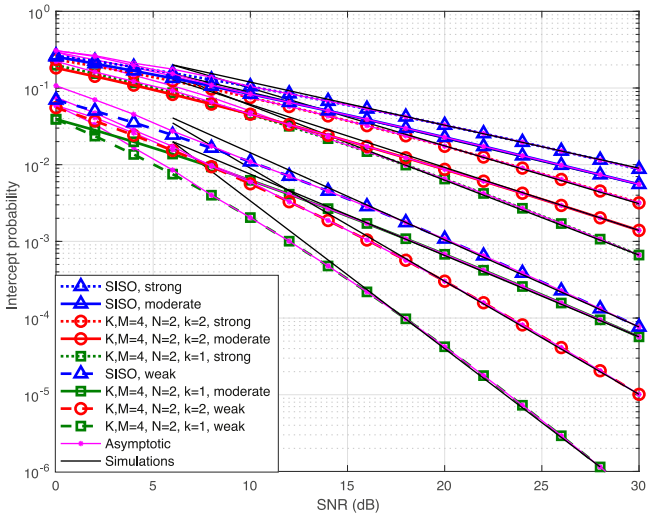

Fig. 9. Intercept probability versus $\bar{\gamma}_r$ for selected K, M, N values.

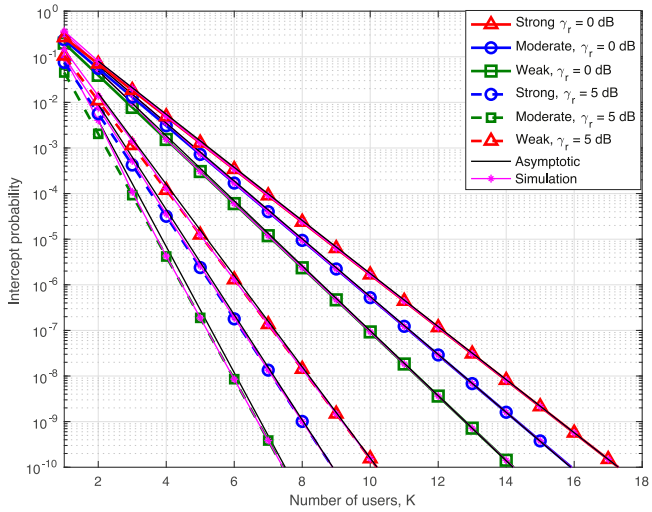

Fig. 10. Intercept probability versus K of the FSO system for selected values of $\bar{\gamma}_r$.

and $s = 1$, the system gained about 6 dB with $a = 10$ cm in comparison with the case of $a = 5$ cm when BER $=10^{-5}$. Nevertheless, the analytical curves agree with the simulation curves in the high SNR region, but, the analytical results depart from the simulation results in the low SNR region as clearly shown in this figure.

Next, we investigate the effects of system and channel parameters on the security performance of the MU-MIMO FSO. Fig. 9 presents the security performance represented by the intercept probability as a function of the average SNR in dB for legitimate $T \rightarrow R$ links with $\bar{\gamma}_e = 10$ dB, $K, P = 4$, and $(\sigma_x/a,\ \sigma_y/a) =$ (9,7) with different M, N, k numbers and varying atmospheric turbulence conditions. First, we find that the values of the interception probability decrease with increasing M and N at all turbulence strengths. Moreover, the intercept probability decreases linearly with increasing of SNR values, indicating a linear relationship between diversity order and SNR. The results also show that the case of $M, N,\ k =$ (4, 2, 1) performs best under weak turbulence. A continuous decrease in the strength of turbulence on the FSO links would lead to a significant decrease in the intercept probability values. For example, when $M, N, k =$ (4, 2, 1), the MU-MIMO system achieves a P_{int} of 10^{-6} in weak turbulence with $\bar{\gamma}_r = 28$ dB, which increases to 1.3×10^{-4} in the case of the SISO system and the same turbulence condition. The agreement between the analytical and simulation curves at high SNR values proves the accuracy of our analysis.

Now we will demonstrate the impact of the number of users and the average SNR of the $T \rightarrow R$ links on the security performance of the considered system, as shown in Fig. 10. In this case, we set the number of P to 4 and $(\sigma_x/a,\ \sigma_y/a) =$ (9,7). It can be observed that the performance of P_{int} with a large value of $\bar{\gamma}_r$ is superior to that with a low value of $\bar{\gamma}_r$ at all turbulence strengths. Moreover, the P_{int} decreases with increasing K. This is because as K increases, the legitimate links between the T and R increase, improving the overall SNR value of the receiver and thus decreasing the P_{int} value. However, as expected, the system performs better in weak and moderate turbulence than in strong turbulence.

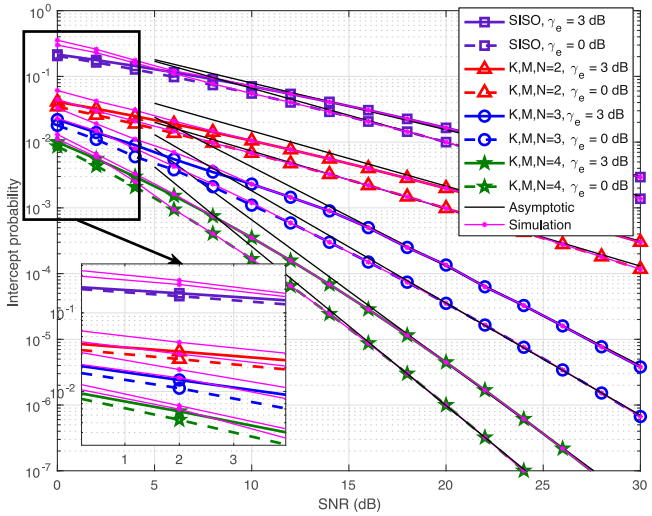

Fig. 11. Intercept probability versus $\bar{\gamma}_r$ for selected values of $K,\ M,\ N$, and $\bar{\gamma}_e$.

Fig. 11 illustrates the combined effects of the number of users, number of apertures, and SNR of $T \rightarrow E$ links on the intercept probability of the investigated system. In this case, a strong turbulence strength, $(\sigma_x/a,\ \sigma_y/a) =$ (9,7), and $P =$ 4 are considered. The system achieves lower P_{int} with higher $K,\ M$, and N. This outcome can be explained by the high power received by R when $K,\ M$, and N increase. When $\bar{\gamma}_e = 3$ dB, the system's performance is worse than the P_{int} at $\bar{\gamma}_e = 0$ dB because the $T \rightarrow E$ link receives more power in this case.

From the previous results in Figs. 3–11, it can be deduced that the simulations and the asymptotic results agree well with the exact results at high SNR values, which proves the accuracy of the expressions derived previously in Sections IV, V, and VI. However, the curves deviate from each other at low SNR regimes due to the approximation of (8).

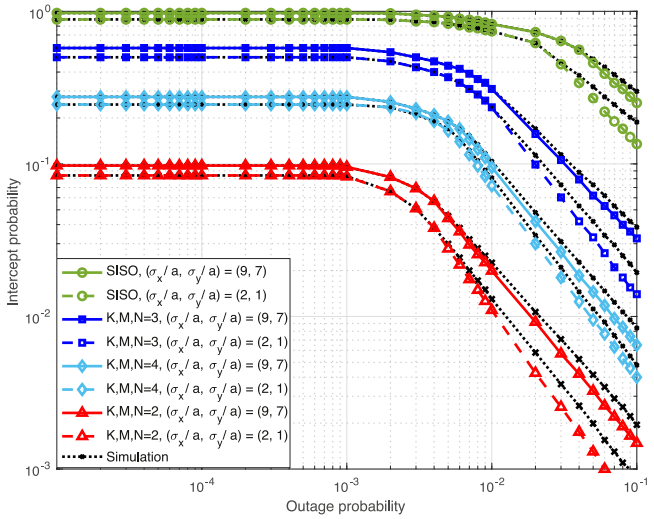

Fig. 12. Intercept probability versus outage probability for selected values of K, M, N considering pointing errors.

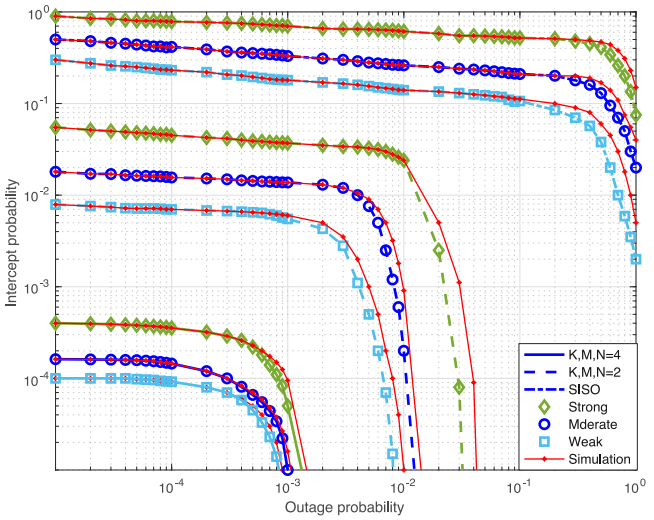

Fig. 13. Intercept probability versus outage probability for selected values of K, M, N, considering atmospheric turbulence.

In the following, we will discuss the combined effect of turbulence, generalized nonzero boresight pointing errors, the number of users, and the number of eavesdroppers' apertures on the SRT of the system under consideration in Figs. 12 and 13. Fig. 12 shows the effects of generalized pointing errors on the SRT of the system in the presence of strong turbulence and $P = 4$. In this case, we set $\bar{\gamma}_r$ and $\bar{\gamma}_e$ to 5 dB. The numerical results show that the intercept probability decreases with the deterioration of P_{out}, indicating the close relationship between the two indicators. However, when the value of jitter is low $(\sigma_x/a,\ \sigma_y/a) = (2, 1)$ and the number of K, M, N is high, the system has better performance because the received power by R is increased, which leads to a decrease in the interception probability. Moreover, with the adopted TAS scheme, the MU-MIMO system performs better than the SISO system. Additionally, a good match between analytical and simulation results can be seen at high values of P_{out} and P_{int}.

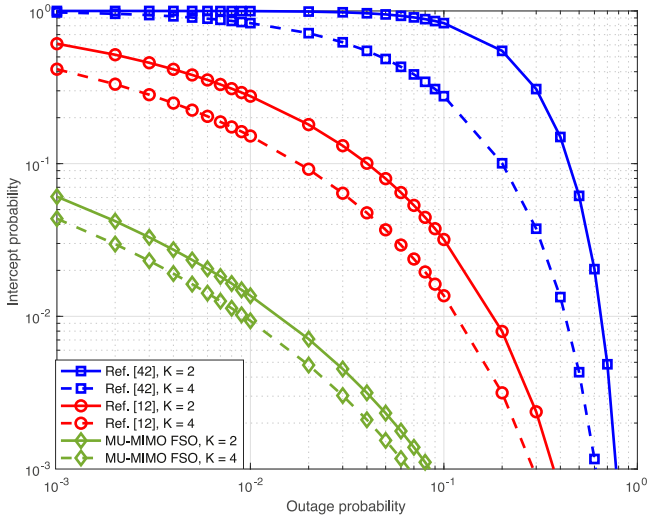

Fig. 14. Intercept probability versus outage probability for selected values of K.

In Fig. 13, we display the SRT of the system under consideration for different numbers of $K, M,\ N$, with $P = 4$. In this case, we assume $\bar{\gamma}_r = \bar{\gamma}_e = 5$ dB, with $(\sigma_x/a,\ \sigma_y/a) =$ (9,7). Fig. 13 shows that the SRT improves under all turbulence conditions when $K,\ M$, and N increase from 2 to 4. However, as expected, the intercept and outage probability results under weak turbulence conditions are better than those under moderate and strong turbulence conditions. Additionally, the agreement between the analytical and simulation results at high values of P_{out} and P_{int} shows the accuracy of our SRT analysis.

Further, we have considered the models used in [12], and [42] to compare the results under moderate turbulence condition, $\bar{\gamma}_r = \bar{\gamma}_e = 5$ dB, and $(\sigma_x/a,\ \sigma_y/a) =$ (9,7). This comparison is shown in Fig. 14. It can be observed that the results obtained for the considered MU-MIMO FSO system is superior to the models used in [12], and [42].

The general observation of the previous results shows that increasing the number of users K resulted in an increase in the number of links between the T and the legitimate receiver R, which improves the overall SNR value of the receiver and thus improves the overall system performance including the outage probability, the interception probability, and the SRT, as demonstrated in (20), (38), and (43).

VIII. Conclusion

We examined the performance of the MU-MIMO FSO system using TAS opportunistic scheme, which utilizes the best user selection by the authorized receiver. The outage probability, average BER, intercept probability, and SRT closed-form expressions were developed based on the adopted power series expansion of the Meijer-G function, assuming a generalized Malaga-M distribution and nonzero boresight pointing errors for MIMO FSO links. In addition, an asymptotic closed-form expression for the outage probability, average BER, intercept probability, and SRT was also derived for high SNR values. The proposed analysis sheds substantial light on the secrecy performance of the MU-MIMO FSO system in the presence of

eavesdropper attacks using the developed expressions for the interception probability. The main findings of this work show that increasing the number of users and the number of apertures of the transmitter and receiver improves the system performance regardless of channel conditions. Moreover, the simulations and the asymptotic results agree well with the exact results at high SNR values showing the accuracy of the obtained expressions. Finally, the adopted TAS scheme of the MU-MIMO FSO system provided significant improvement in security, reliability, and SRT performance compared to the SISO FSO system.

REFERENCES

[1] I. Union, "IMT traffic estimates for the years 2020 to 2030," ITU, Rep. 2370, 2015.

[2] R. Boluda-Ruiz, A. García-Zambrana, B. Castillo-Vázquez, and K. Qaraqe, "Secure communication for FSO links in the presence of eavesdropper with generic location and orientation," *Opt. Exp.*, vol. 27, no. 23, pp. 34211–34229, 2019.

[3] W. M. R. Shakir, "Performance evaluation of a selection combining scheme for the hybrid FSO/RF system," *IEEE Photon. J.*, vol. 10, no. 1, Feb. 2018, Art. no. 7901110.

[4] A. Jahid, M. H. Alsharif, and T. J. Hall, "A contemporary survey on free space optical communication: Potentials, technical challenges, recent advances and research direction," *J. Netw. Comput. Appl.*, vol. 200, 2022, Art. no. 103311.

[5] P. V. Trinh, A. Carrasco-Casado, A. T. Pham, and M. Toyoshima, "Secrecy analysis of FSO systems considering misalignments and eavesdropper's location," *IEEE Trans. Commun.*, vol. 68, no. 12, pp. 7810–7823, Dec. 2020.

[6] W. M. R. Shakir and S. A. A. Mohammed, "Free space optical communications security and reliability trade-off: A survey," in *Proc. Int. Conf. Natural Appl. Sci.*, 2022, pp. 114–119.

[7] H. Wu et al., "Secrecy performance analysis in the FSO communication system considering different eavesdropping scenarios," *Opt. Exp.*, vol. 30, no. 23, pp. 41028–41047, 2022.

[8] Y. Ai, A. Mathur, G. D. Verma, L. Kong, and M. Cheffena, "Comprehensive physical layer security analysis of FSO communications over Málaga channels," *IEEE Photon. J.*, vol. 12, no. 6, Dec. 2020, Art. no. 7906617.

[9] W. M. R. Shakir and R. A. Abdulkareem, "A survey on physical layer security for FSO communication systems," in *Proc. Int. Multi-Disciplinary Conf. Integr. Sci. Technol.*, 2021, pp. 180–191.

[10] M. E. P. Monteiro, J. L. Rebelatto, R. D. Souza, and G. Brante, "Effective secrecy throughput analysis of relay-assisted free-space optical communications," *Phys. Commun.*, vol. 35, 2019, Art. no. 100731.

[11] R. Boluda-Ruiz, S. C. Tokgoz, A. García-Zambrana, and K. Qaraqe, "Enhancing secrecy capacity in FSO links via MISO systems through turbulence-induced fading channels with misalignment errors," *IEEE Photon. J.*, vol. 12, no. 4, Aug. 2020, Art. no. 7903313.

[12] W. M. R. Shakir, "On secrecy performance of multiuser FSO networks with opportunistic user scheduling," in *Proc. Int. Symp. Netw., Comput. Commun.*, 2021, pp. 1–6.

[13] A. Sikri, A. Mathur, and G. Verma, "Secrecy performance enhancement of artificial noise injection scheme-based FSO systems," in *Proc. IEEE 94th Veh. Technol. Conf.*, 2021, pp. 01–05.

[14] G. Narang, M. Aggarwal, H. Kaushal, and S. Ahuja, "Enhancing the security of free space optical communication system by employing chaos-based modulation scheme," *J. Opt. Commun.*, pp. 1–12, 2023.

[15] F. J. Lopez-Martinez, G. Gomez, and J. M. Garrido-Balsells, "Physical layer security in free-space optical communications," *IEEE Photon. J.*, vol. 7, no. 2, Apr. 2015, Art. no. 7901014.

[16] M. J. Saber and S. M. S. Sadough, "On secure free-space optical communications over Malaga turbulence channels," *IEEE Wireless Commun. Lett.*, vol. 6, no. 2, pp. 274–277, Apr. 2017.

[17] G. D. Verma, A. Mathur, Y. Ai, and M. Cheffena, "Secrecy performance of FSO communication systems with non-zero boresight pointing errors," *IET Commun.*, vol. 15, no. 1, pp. 155–162, 2021.

[18] M. E. P. Monteiro, J. L. Rebelatto, R. D. Souza, and G. Brante, "Maximum secrecy throughput of MIMOME FSO communications with outage constraints," *IEEE Trans. Wireless Commun.*, vol. 17, no. 5, pp. 3487–3497, May 2018.

[19] L. Han, Y. Wang, X. Liu, and B. Li, "Secrecy performance of FSO using HD and IM/DD detection technique over F-distribution turbulence channel with pointing error," *IEEE Wireless Commun. Lett.*, vol. 10, no. 10, pp. 2245–2248, Oct. 2021.

[20] W. M. R. Shakir, "Performance analysis of the hybrid MMW RF/FSO transmission system," *Wireless Pers. Commun.*, vol. 109, pp. 2199–2211, 2019.

[21] A. Asadi and V. Mancuso, "A survey on opportunistic scheduling in wireless communications," *IEEE Commun. Surv. Tut.*, vol. 15, no. 4, pp. 1671–1688, Fourth Quarter 2013.

[22] J. G. Andrews, A. Ghosh, and R. Muhamed, *Fundamentals of WiMAX: Understanding Broadband Wireless Networking*. Englewood Cliffs, NJ, USA: Prentice-Hall, 2007.

[23] S. Sharma, J. Tan, A. S. Madhukumar, and R. Swaminathan, "Switching-based transmit antenna/aperture selection in a MISO hybrid FSO/RF system," in *Proc. IEEE Glob. Commun. Conf.*, 2018, pp. 1–6.

[24] Y. Zou, X. Wang, W. Shen, and L. Hanzo, "Security versus reliability analysis of opportunistic relaying," *IEEE Trans. Veh. Technol.*, vol. 63, no. 6, pp. 2653–2661, Jul. 2014.

[25] X. Ding, Y. Zou, F. Ding, D. Zhang, and G. Zhang, "Opportunistic relaying against eavesdropping for Internet-of-Things: A security-reliability trade-off perspective," *IEEE Internet Things J.*, vol. 6, no. 5, pp. 8727–8738, Oct. 2019.

[26] J. Ji, B. Wu, J. Zhang, M. Xu, and K. Wang, "Enhancement of reliability and security in a time-diversity FSO/CDMA wiretap channel," *OSA Continuum*, vol. 2, no. 5, pp. 1524–1538, 2019.

[27] N. Alshaer, A. Moawad, and T. Ismail, "Reliability and security analysis of an entanglement-based QKD protocol in a dynamic ground-to-UAV FSO communications system," *IEEE Access*, vol. 9, pp. 168052–168067, 2021.

[28] J. Abouei and K. N. Plataniotis, "Multiuser diversity scheduling in free-space optical communications," *J. Lightw. Technol.*, vol. 30, no. 9, pp. 1351–1358, May 2012.

[29] L. Yang, X. Gao, and M.-S. Alouini, "Performance analysis of free-space optical communication systems with multiuser diversity over atmospheric turbulence channels," *IEEE Photon. J.*, vol. 6, no. 2, Apr. 2014, Art. no. 7901217.

[30] S. Zhalehpour and M. Uysal, "Performance of multiuser scheduling in free space optical systems over atmospheric turbulence channels," *IET Optoelectron.*, vol. 9, no. 5, pp. 275–281, 2015.

[31] S. Zhalehpour, M. Uysal, O. A. Dobre, and T. Ngatched, "Outage capacity and throughput analysis of multiuser FSO systems," in *Proc. IEEE 14th Can. Workshop Inf. Theory*, 2015, pp. 143–146.

[32] M. Qin, L. Chen, and W. Wang, "Generalized selection multiuser scheduling for the MIMO FSO communication system and its performance analysis," *IEEE Photon. J.*, vol. 8, no. 5, Oct. 2016, Art. no. 7906609.

[33] N. Cherif, I. Trigui, and S. Affes, "On the performance analysis of mixed multi-aperture FSO/multiuser RF relay systems with interference," in *Proc. IEEE 18th Int. Workshop Signal Process. Adv. Wireless Commun.*, 2017, pp. 1–5.

[34] A. M. Salhab, F. S. Al-Qahtani, R. M. Radaydeh, S. A. Zummo, and H. Alnuweiri, "Power allocation and performance of multiuser mixed RF/FSO relay networks with opportunistic scheduling and outdated channel information," *J. Lightw. Technol.*, vol. 34, no. 13, pp. 3259–3272, Jul. 2016.

[35] Y. F. Al-Eryani, A. M. Salhab, S. A. Zummo, and M.-S. Alouini, "Performance analysis and power allocation for two-way multi-user mixed RF/FSO relay networks," in *Proc. IEEE Wireless Commun. Netw. Conf.*, 2018, pp. 1–6.

[36] M. A. Amer and S. Al-Dharrab, "Performance of two-way relaying over α-μ fading channels in hybrid RF/FSO wireless networks," 2019, *arXiv:1911.05959*.

[37] I. Trigui, S. Affes, A. M. Salhab, and M.-S. Alouini, "Transmit diversity for FSO/RF-based multiuser networks," in *Proc. Int. Wireless Commun. Mobile Comput.*, 2020, pp. 1118–1123.

[38] J. Zhang, H. Ran, G. Pan, and Y. Xie, "Outage probability of multi-aperture and multi-antenna wireless-powered relaying assisted FSO-RF systems with a nonlinear energy harvester," *Appl. Opt.*, vol. 59, pp. 10269–10277, 2020.

[39] P. K. Singya and M.-S. Alouini, "Performance of UAV assisted multiuser terrestrial-satellite communication system over mixed FSO/RF channels," *IEEE Trans. Aerosp. Electron. Syst.*, vol. 58, no. 2, pp. 781–796, 2022.

[40] E. T. Michailidis, P. S. Bithas, N. Nomikos, D. Vouyioukas, and A. G. Kanatas, "Outage probability analysis in multi-user FSO/RF and UAV-enabled MIMO communication networks," *Phys. Commun.*, vol. 49, 2021, Art. no. 101475.

[41] C. Abou-Rjeily, "Performance analysis of FSO communications with diversity methods: Add more relays or more apertures?," *IEEE J. Sel. Areas Commun.*, vol. 33, no. 9, pp. 1890–1902, Sep. 2015.

[42] A. H. Abd El-Malek, A. M. Salhab, S. A. Zummo, and M.-S. Alouini, "Security-reliability trade-off analysis for multiuser SIMO mixed RF/FSO relay networks with opportunistic user scheduling," *IEEE Trans. Wireless Commun.*, vol. 15, no. 9, pp. 5904–5918, Sep. 2016.

[43] A. H. Abd El-Malek, A. M. Salhab, S. A. Zummo, and M.-S. Alouini, "Physical layer security enhancement in multiuser mixed RF/FSO relay networks under RF interference," in *Proc. IEEE Wireless Commun. Netw. Conf.*, 2017, pp. 1–6.

[44] H. Lei et al., "On secure mixed RF-FSO systems with TAS and imperfect CSI," *IEEE Trans. Commun.*, vol. 68, no. 7, pp. 4461–4475, Jul. 2020.

[45] G. K. Varotsos, H. E. Nistazakis, M. I. Petkovic, G. T. Djordjevic, and G. S. Tombras, "SIMO optical wireless links with nonzero boresight pointing errors over M-modeled turbulence channels," *Opt. Commun.*, vol. 403, pp. 391–400, 2017.

[46] A. Das, B. Bag, C. Bose, and A. Chandra, "Free space optical links over Málaga turbulence channels with transmit and receive diversity," *Opt. Commun.*, vol. 456, 2020, Art. no. 124591.

[47] H. E. A. Jurado-Navas, J. M. Garrido-Balsells, J. F. Paris, and A. Puerta-Notario, "A unifying statistical model for atmospheric optical scintillation," in *Numerical Simulations of Physical and Engineering Processes*. London, U.K.: IntechOpen, 2011, ch. 8, pp. 181–205.

[48] L. C. Andrews and R. L. Phillips, *Laser Beam Propagation Through Random Media*, vol. 52. Bellingham, WA, USA: SPIE, 2005.

[49] P. V. Trinh, T. V. Phamm, and A. T. Pham, "Free-space optical systems over correlated atmospheric fading channels: Spatial diversity or multihop relaying?," *IEICE Trans. Commun.*, vol. E101.B, no. 9, pp. 2033–2046, 2018.

[50] The Wolfram Functions Site, 2008. [Online]. Available: http://functions.wolfram.com/Bessel-TypeFunctions/BesselK/06/ShowAll.html

[51] Y. Dhungana and C. Tellambura, "New simple approximations for error probability and outage in fading," *IEEE Commun. Lett.*, vol. 16, no. 11, pp. 1760–1763, Nov. 2012.

[52] H. A. David and H. N. Nagaraja, *Order Statistics*. Hoboken, NJ, USA: Wiley, 1981.

[53] Y. Ma, J. Jin, and D. Zhang, "Throughput and channel access statistics of generalized selection multiuser scheduling," *IEEE Trans. Wireless Commun.*, vol. 7, no. 8, pp. 2975–2987, Aug. 2008.

[54] I. Trigui, S. Affes, A. M. Salhab, and M.-S. Alouini, "Multi-user mixed FSO-RF systems with aperture selection under Poisson field interference," *IEEE Access*, vol. 7, pp. 73764–73781, 2019.

[55] Y. Ma and S. Pasupathy, "Efficient performance evaluation for generalized selection combining on generalized fading channels," *IEEE Trans. Wireless Commun.*, vol. 3, no. 1, pp. 29–34, Jan. 2004.

[56] I. S. Gradshteyn and I. M. Ryzhik, *Table of Integrals, Series, and Products*, 7th ed. New York, NY, USA: Academic, 2007.

[57] W. M. R. Shakir and R. A. A. Abdul Kareem, "On secure communications for FSO systems over generalized turbulence channels," in *Proc. IEEE Int. Symp. Meas. Netw.*, 2022, pp. 1–6.

[58] A. P. Prudnikov, Y. A. Brychkov, and O. I. Marichev, *Integrals and Series—Vol. 3: More Special Functions*. New York, NY, USA: Gordon & Breach, 2003.

[59] I. Wolfram, Mathematical Edition: Version 8.0. Champaign, Illinois, USA: Wolfram Research Inc., 2010. [Online]. Available: http://functions.wolfram.com

[60] A. A. Kilbas, *H-Transforms: Theory and Applications*. Boca Raton, FL, USA: CRC Press, 2004.

[61] I. S. Ansari, S. Al-Ahmadi, F. Yilmaz, M.-S. Alouini, and H. Yanikomeroglu, "A new formula for the BER of binary modulations with dual-branch selection over generalized-K composite fading channels," *IEEE Trans. Commun.*, vol. 59, no. 10, pp. 2654–2658, Oct. 2011.

[62] M. R. Bhatnagar and Z. Ghassemlooy, "Performance analysis of Gamma-Gamma fading FSO MIMO links with pointing errors," *J. Lightw. Technol.*, vol. 34, no. 9, pp. 2158–2169, May 2016.

[63] S. Sharma, A. Madhukumar, and S. R, "MIMO hybrid FSO/RF system over generalized fading channels," *IEEE Trans. Veh. Technol.*, vol. 70, no. 11, pp. 11565–11581, Nov. 2021.

[64] M. R. Bhatnagar, "A one bit feedback based beamforming scheme for FSO MISO system over Gamma-Gamma fading," *IEEE Trans. Commun.*, vol. 63, no. 4, pp. 1306–1318, Apr. 2015.

[65] E. Illi, F. El Bouanani, D. B. da Costa, F. Ayoub, and U. S. Dias, "Dual-hop mixed RF-UOW communication system: A PHY security analysis," *IEEE Access*, vol. 6, pp. 55345–55360, 2018.